INTERNATIONAL ATOMIC ENERGY AGENCY
UNITED NATIONS EDUCATIONAL, SCIENTIFIC AND CULTURAL ORGANIZATION

INTERNATIONAL CENTRE FOR THEORETICAL PHYSICS
34100 TRIESTE (ITALY) - P.O.B. 586 - MIRAMARE - STRADA COSTIERA 11 - TELEPHONE: 2240-1
CABLE: CENTRATOM - TELEX 460392 - 1

SMR/388 - 38

SPRING COLLEGE IN MATERIALS SCIENCE
ON
'CERAMICS AND COMPOSITE MATERIALS'
(17 April - 26 May 1989)

MECHANICAL BEHAVIOUR OF COMPOSITES
(Background Material)

O. SBAIZERO
Istituto di Chimica Applicata ed Industriale
Cerimacs
Via Valerio, 2
34127 Trieste
Italy

MATERIALS

THE MECHANICAL PERFORMANCE OF FIBER REINFORCED CERAMIC MATRIX COMPOSITES

by

A. G. Evans
Materials Department
College of Engineering
University of California
Santa Barbara, California 93106

and

D. B. Marshall
Rockwell International Science Center
1049 Camino Dos Rios
Thousand Oaks, California 91360

M88-18

ABSTRACT

This article evaluates the current understanding of relationships between microstructure and mechanical properties in ceramics reinforced with aligned fibers. Emphasis is placed on definition of the micromechanical properties of the interface that govern the composite toughness. Issues such as the debond and sliding resistance of the interface are discussed based on micromechanics calculations and experiments conducted on both model composites and actual composites.

TABLE OF CONTENTS

NOTATION

α	linear thermal expansion coefficient
ε	stress-free strain ($\Delta\alpha\Delta T$): positive refers to residual compression normal to the interface
μ	friction coefficient
ν	Poisson's ratio of composite
ξ	coefficient = $(1-f)[(1-f)(1-\nu+\nu\Sigma)+\Sigma(1-f)]$
Σ	ratio of Young's modulus of fiber to matrix, E^f/E^m.
σ_0	matrix cracking stress
σ_u	ultimate strength
σ_∞	applied stress
σ^c	stress for transverse interface failure
τ	shear resistance of interface after debonding
$\Phi(h)$	cumulative pull-out distribution
ϕ	crack surface shear angle
$\phi(z, t)$	probability density function for fiber failure
χ	interface fracture parameter = $EH^2/\mathcal{G}_0L$
ψ	phase angle of loading
a	Dundurs' parameter = $\dfrac{G_1(1-\nu_2)-G_2(1-\nu_1)}{G_1(1-\nu_2)+G_2(1-\nu_1)}$
B	Transition parameter

b	Dundurs' parameter $= \frac{G_1(1-2\nu_2) - G_2(1-2\nu_1)}{2[G_1(1-\nu_2) + G_2(1-\nu_1)]}$
D	matrix crack spacing
d	debond length
E	Young's modulus of composite
F	non-dimensional stress $= (t-p)/E^f\varepsilon$
f	fiber volume fraction
G	shear modulus
$\mathcal{G}$	strain energy release rate
$\mathcal{G}_{ic}$	critical strain energy release rate for interface
$\mathcal{G}_{ss}$	steady-state strain energy release rate
$\mathcal{G}_{fc}$	critical strain energy release rate for the fiber
$\mathcal{G}_{Mc}$	critical strain energy release rate for the composite
$\mathcal{G}_{0c}$	intrinsic critical strain energy release rate for the interface
$\mathcal{G}_R(\Delta a)$	increase in critical strain energy release rate with increase in crack length, Δa.
H	amplitude of interface roughness
h	pull-out length
ℓ	slip length
L	gauge length
m	shape parameter for fiber strength distribution
p	residual axial stress in the matrix $= \frac{\lambda_2}{\lambda_1}\left(\frac{E'}{E}\right)\frac{f\varepsilon E^M}{1-\nu^M}$
q	residual compression normal to interface $= (1-f)E^M\varepsilon/2\lambda_1(1-\nu^M)$
R	fiber radius

r	distance from crack front
S	fiber strength
S_o	scale parameter for fiber strength distribution
T	pull-out parameters
t	stress acting on fiber between crack surfaces
U	pull-out parameter $= T^2R/4E^f\tau(1+\xi)$
u	crack opening displacement
v	crack shear displacement
z	distance from crack plane

I INTRODUCTION

Practical ceramic matrix composites reinforced with continuous fibers exhibit important failure/damage behaviors in mode I, mode II and mixed mode I/II, as well as in compression. The failure sequence depends on whether the reinforcement is uniaxial or multiaxial and whether woven or laminated architectures are used. However, the underlying failure processes are fully illustrated by the behavior of uniaxially reinforced systems. The basic features are sketched in Fig. 1. The intent of the present article is to provide an assessment of relationships between the properties of the constituents (fiber, matrix, interface) and the overall mechanical performance of the composite. At the outset, it is recognized that the composite properties are dominated by the interface, such that upper bounds must be placed on the interface debond and sliding resistance in order to have a composite with attractive mechanical properties. A major emphasis of the article thus concerns the definition of optimum properties for coatings and interphases between the fibers and the matrix, subject to high temperature stability and integrity. Residual stresses in the composite caused by thermal expansion differences are also very important and are confronted throughout.

The strong dependence of ceramic matrix composite properties on the mechanical properties of the interface generally demands consideration of fiber coatings and/or reaction product layers, at least for high temperature use. Thus, while composites fabricated using low temperature matrix infiltration procedures, such as chemical vapor infiltration (CVI), can create composites that exhibit limited interface bonding and, therefore, have acceptable ambient temperature properties, experience indicates that moderate temperature exposure causes diffusion, coupled with the ingress of O_2, N_2, etc., from the environment, resulting in chemical bonding across the interface. The resultant interphase consisting of oxides, nitrides,

carbides (either separately or in combination) invariably have sufficiently high fracture resistance that desirable composite properties are not retained. Consequently, a major objective of this article and of continuing research on ceramic matrix composites is the identification of interphases that are both stable at high temperature and bond poorly to either the fiber or the matrix. Certain refractory metals and intermetallics seem to have these attributes, as elaborated in the following chapters.

The basic philosophy of this article is that the overall mechanical behavior is sufficiently complex and involves a sufficiently large number of independent variables that empiricism is an inefficient approach to microstructure optimization. Instead, optimization only becomes practical when each of the important damage and failure modes has been described by a rigorous model, validated by experiment. The coupling between experiment and theory is thus a prevalent theme. It is also noted that this objective can only be realized if the models are based on homogenized properties that describe representative composite elements, while also taking into account the constituent properties of the fibers, matrix and interface. Models that attempt to discretize microstructural details have little merit in the context of the above objective. In this regard, the present philosophy is analogous to that used successfully to describe process zone phenomena such as transformation and microcrack toughening,[1-5] as well as ductile fracture,[6,7] wherein the behavior of individual particles, dislocations, etc., provides input to the derivation of constitutive properties that describe the continuum behavior.

The behavior of the composite is intimately coupled to some basic features of crack propagation and sliding along interfaces. Indeed, the response of the composite can be simulated by studying interface responses in judiciously selected test specimens. The basic mechanics and the implications of tests used to study interface debonding and sliding are presented first. The characteristics of the

damage and fracture processes that occur in each of the important modes depicted in Fig. 1 are then described. Finally, implications for the choice of matrices, fibers and coatings that provide good mechanical properties are discussed.

II INTERFACE DEBONDING AND SLIDING

1. MECHANICS OF INTERFACE CRACKS

Interface debonding in ceramic matrix composites occurs both at the matrix crack front and in the crack wake (Fig. 2). Both processes are mixed mode. Furthermore, debond cracks typically occur between materials (fiber, matrix, coating) having quite different elastic properties. The requisite mechanics thus concern cracks on bimaterial interfaces, resulting in a more complex fracture mechanics formulism than the familiar stress intensity factors used in elastically homogeneous systems. The additional features that need to be introduced when considering interface cracks derive from the fact that the mixity of opening and shearing of the surface depends on the modulus mismatch and on the crack length, as well as on the mode of loading. Consequently, the debond resistance of a bimaterial interface must always be characterized by two parameters: the critical strain energy release rate, $\mathcal{G}_{ic}$, and the phase angle of loading, ψ (Fig. 3). The latter quantity is somewhat dependent on the choice of units, for reasons elaborated elsewhere.[8] However, this presents no difficulty, provided that a consistent choice is made. The strain energy release rate, $\mathcal{G}$, and the phase angle can be calculated for any problem of interest and can be expressed in terms of the applied loads, specimen dimensions and debond length.

The basic relationship used to calculate $\mathcal{G}$ and ψ can be defined with reference to Fig. 4. The phase angle is related to the angle of rotation ϕ of the crack surface as the crack opens by;[8,9]

$$\psi = \phi - (1/2\pi)\ln[(1-b)/(1+b)] \tag{1}$$

with b being one of the Dundurs' parameters[10] (a and b);

$$a = [G_1(1-\upsilon_2) - G_2(1-\upsilon_1)]/[G_1(1-\upsilon_2) + G_2(1-\upsilon_1)]$$

$$b = \left(\frac{1}{2}\right)[G_1(1-2\upsilon_2) - G_2(1-2\upsilon_1)]/[G_1(1-\upsilon_2) + G_2(1-\upsilon_1)] \tag{2}$$

G is the shear modulus, υ is Poisson's ratio and r is the distance from the crack front. The energy release rate is related to the crack surface displacements (u, v) by;[8,9]

$$\mathcal{G} = \frac{\pi\left(1+4[\ln[(1-b)/(1+b)]/2\pi]^2\right)(u^2+v^2)}{8r[(1-\upsilon_1)/G_1 + (1-\upsilon_2)/G_2]} \tag{3}$$

where the fiber and matrix have essentially the same elastic properties, $\mathcal{G}$ can be related to the stress intensity factor, K, in the usual manner, $K^2 = E\mathcal{G}/(1-\upsilon^2)$.

2. DEBONDING MECHANICS

Debonding solutions are required for axisymmetric loading, representative of the debonding of fibers (Fig. 2), as well as for planar cracks characteristic of macroscopic delamination (Fig. 1). In both cases, $\mathcal{G}$ and ψ are strongly influenced by

the residual stress. Furthermore, when the phase angle becomes large, $\psi \rightarrow \pi/2$, frictional sliding and crack surface locking effects become important.[11] A comprehensive set of solutions that fully encompass the spectrum of residual stress and of frictional sliding relevant to composites does not yet exist. The known solutions are described below.

Axisymmetric solutions exist for composites with interfaces subject to residual radial tension, wherein a net crack opening exists for the full range of applied loads, elastic moduli and fiber volume fractions.[12] All solutions have the general features that $\mathcal{G}$ is small, but non-zero, when the debond length is zero and increases to a steady-state value $\mathcal{G}_{ss}$ when the debond length d exceeds ~R (Fig. 5a). Such behavior indicates the insightful bound that the debond must extend without limit when $\mathcal{G}_{ss}$ exceeds $\mathcal{G}_{ic}$ at the appropriate ψ (see Fig. 3). The basic trends in $\mathcal{G}_{ss}$ and ψ relevant to wake debonding, determined using finite elements, are summarized in Figs. 5b, c. The variables in the analysis are: the ratio Σ of Young's modulus for the fiber, E^f, the test of the matrix, E^m, the fiber volume fraction, f, the stress-free (residual) strain ε, the stress imposed on the fiber, t, and the Poisson's ratios υ^m and υ^f. Note that the phase angles are typically large, indicative of a large ratio of shear to opening.

Rigorous axisymmetric solutions for interfaces subject to residual radial compression have not been derived. However, some approximate solutions based on a modified shear lag approach are insightful.[13] This approach has merit when the friction coefficient μ is small ($\mu \lesssim 0.2$). For this case, crack opening does not occur until t reaches a critical value t_c given by;

$$t_c/E^f\varepsilon = 1/\upsilon^f \tag{4}$$

For $t > t_c$, steady-state obtains for long debonds and the solutions given in Fig. 5 are directly applicable. For $t < t_c$, the debond crack is subject to normal compression and $\mathcal{G}$ diminishes with increase in debond length, d, representative of λ stable debonds,

$$\mathcal{G}/E^fR\varepsilon^2 = F^2 + 2F - \frac{4\mu d(1-f)(1+F)(1-\upsilon F)}{R[1+f+(1-f)(1-2\upsilon)]} \tag{5}$$

where

$$F = (t-p)/E^f\varepsilon$$

$$\xi = (1-f)/[(1-f)(1-2\nu)+\Sigma(1-f)]$$

for $\nu^f = \nu^m = \nu$ and p is the axial residual stress in the matrix as governed by ε, f and Σ. The $\mathcal{G}$ in this instance is strictly mode II and debonding should thus be predicted by equating $\mathcal{G}$ to $\mathcal{G}_{ic}$ at $\psi = \pi/2$. Such predictions have not been attempted. However, it is insightful to note that, for "weak" interfaces ($\mathcal{G}_{ic} << \mathcal{G}_{fc}$), the debond length and the slip length, ℓ, are likely to be closely related, with ℓ given by;[13]

$$\ell/R = t/2E^f\varepsilon\mu\xi(1-\nu^fF) \tag{6}$$

For the plane delamination problem depicted in Fig. 1, a comprehensive analysis exists,[14] expressible in terms of imposed axial forces and bending moments. The solution having greatest relevance to problems in ceramic matrix composites involves the four-point bending of a bimaterial beam with debond cracks between the inner loading points.[9,14] The general form of the solution (Fig. 6a) indicates that $\mathcal{G}$ has a maximum upon initial debonding and then decays to a steady-state level

when d exceeds the thickness of the upper (matrix) layer by ~ 3. Such behavior suggests that initial debonding occurs stably, but then becomes unstable. Trends in the steady-state value $\mathcal{G}_{ss}$ are summarized in Fig. 6b. The corresponding non-dimensional phase angle, ψ^* is ~ 0.68 for all Σ, when $\varepsilon = 0$. Clearly, the elastic properties have strong influences on both $\mathcal{G}_{ss}$ and ψ.

The preceding results also indicate that initial debonding along the interface is expected, provided that $\mathcal{G}_{ic}$ at $\psi = \pi/4$ is less than the critical strain energy release rate for the fiber, $\mathcal{G}_{fc}$, by a ratio that depends on the elastic properties for fiber and matrix. For the elastically homogeneous case, debonding occurs in preference to fiber failure when

$$\mathcal{G}_{ic}/\mathcal{G}_{fc} \lesssim 1/4 \tag{7}$$

Solutions for fibers and matrix having different elastic properties ($\Sigma \neq 1$) do not yet exist. Further crack front debonding is not addressed by this solution. Useful insights concerning this debonding problem can be gained by interpolating between the above mixed mode $\mathcal{G}(\psi)$ solution and $\mathcal{G}_{ic}(O)$ for long, cylindrical debonds in the crack tip field[15] (Fig. 7). The latter solution indicates that debond lengths substantially larger than the fiber diameter result in very small values of $\mathcal{G}_{ic}(O)$ at the interface compared with that the matrix crack front, $\mathcal{G}_{mc}$, as given approximately by;

$$\mathcal{G}_{ic}(O)/\mathcal{G}_{c} = 0.1\,R/d \tag{8}$$

Consequently, it is surmised that the $\mathcal{G}_{ic}(O)$ required for debonding decreases rapidly with debond length, as sketched in Fig. 7. Extensive crack front debonding thus appears unlikely in the absence of residual stress, even when $\mathcal{G}_{ic}$ is quite small.

This conclusion about crack front debonding is substantially changed when residual stress exists. Residual radial tension results in opening mode steady-state interface cracking, characterized by;[12]

$$E'\mathcal{G}_{m} = \pi q^2 R/2 \tag{9}$$

where q is the residual stress normal to the interface, as governed by the stress-free strain, ε, the fiber volume fraction and the elastic properties.[12,15] Superimposing opening mode K's from the residual and applied fields provides a full debonding solution. For elastically homogeneous composites,

$$\mathcal{G}/\mathcal{G}_{m} = \left[0.3\sqrt{\frac{R}{d}} + q\sqrt{\frac{\pi R}{2E\mathcal{G}_{m}}}\right]^2 \tag{10}$$

Equating $\mathcal{G}$ to the critical value for the interface, the debond length becomes

$$d/R = \frac{0.1E\mathcal{G}_{M}/q^2R}{\left[\sqrt{E\mathcal{G}_{i}/q^2R} - \sqrt{\pi/2}\right]^2} \tag{11}$$

As expected, once the debond initiation condition has been satisfied, residual tension encourages further debonding. Indeed, when $q \gtrsim K_i\sqrt{\pi/2R}$, then $d \to \infty$ at the crack front. For this condition, partial debonding is likely upon cooling[16] (See Fig. 10).

Initiation of debonding is a necessary but not sufficient condition for good composite properties. It is also required that the debond crack remain in the interface and not kink into the fiber to cause premature fiber rupture, either along the crack front or in the crack wake. Analysis of this problem[17] (Fig. 8) indicates that

kinking out of the interface is strongly influenced both by the elastic properties of fiber and matrix and by the phase angle. In particular, debond deviation into the fiber is less likely when the fiber has a high modulus: an important rationale for choosing high modulus fibers. Furthermore, even when the fiber has a relatively low modulus, kinking out of the interface is only likely whenever $\mathcal{G}_i(\psi) \lesssim 0.4\ \mathcal{G}_f$.

3. THE INTERFACE FRACTURE RESISTANCE

The preceding mechanics provide the essential background needed for the measurement of debond resistances relevant to composite performance, as summarized in Fig. 9. Three basic test methods have been identified:[9,11,18] compact tension tests, flexural tests and pull-out tests. The former provides data for $\psi = 0$, the latter for $\psi = \pi/2$ and the flexural test for $\psi = \pi/4$. Critical aspects of interface fracture testing concern the initial introduction of a well-defined debond crack and measurement of the residual stress.[18] Another important testing issue concerns friction at the loading points.[19] A procedure that takes frictional effects into account, based on measurements of the hysteresis in loading and unloading compliance has been developed and validated.[19] These rigorous demands on the testing needed to generate valid $\mathcal{G}_i(\psi)$ data, have limited the extent of available results. Preliminary results indicate that $\mathcal{G}_i$ tends to increase with increase in ψ, especially as $\psi \rightarrow \pi/2$, and furthermore, that the rate of increase depends on the morphology of the fracture interface.[11,18] Specifically, rough fracture interfaces cause $\mathcal{G}_i$ to increase more rapidly with increase in ψ (Fig. 3). Analysis of this phenomenon[11] has attributed this trend to the sliding and locking of crack surface asperities that make contact at large phase angles (Fig. 3). The material parameter that governs the magnitude of the above effect is;[11]

$$\chi = EH^2/\mathcal{G}_o L \qquad (12)$$

where H is the amplitude and L the wavelength of undulations on the fracture interface and $\mathcal{G}_o$ is the intrinsic fracture resistance of the interface. Specifically, large χ results in the greatest effects on $\mathcal{G}_i(\psi)$. The quantity χ is a measure of the length of the contact zone, which increases as either H increases or $\mathcal{G}_o$ decreases.

The magnitude of $\mathcal{G}_o$ is clearly influenced by the presence of interphases, the atomistic structure of the interface, etc. However, as yet, residual stress and morphological influences have not been sufficiently decoupled to explore these basic relationships. Nevertheless, preliminary measurements reveal that $\mathcal{G}_o$ is typically quite small for oxides bonded to refractory metals (Nb), to intermetallics (TiAl) and to noble metals (Au, Pt), as well as for oxides bonded with inorganic glasses and for carbides and nitrides having graphite and boron nitride interlayers.

4. DEBONDING DURING COMPOSITE FRACTURE

The preceding debonding results, while still incomplete, are consistent with the following sequence of events during matrix crack propagation. Initial debonding occurs along the interface at the crack front, provided that $\mathcal{G}_f/\mathcal{G}_i$ (at $\psi = \pi/4$) $\gtrsim 4$. The extent of debonding is typically small when residual compression exists at the interface, but can be extensive when the interface is in residual tension. However, more importantly, further debonding is invariably induced in the crack wake.[12] The extent of debonding is again governed largely by the residual field. Residual radial tension results in unstable conditions and encourages extensive debonding.[12] Residual compression causes stable

debonding,[13] with extent determined by the friction coefficient and morphology of the debonded interface. Fracture of the fiber by kinking of the debond crack into the fiber is unlikely,[16] especially when the fiber modulus is relatively large. Fiber failure and pull-out toughening thus appear to be strongly influenced by the statistics of fiber failure.[20]

The above sequence indicates that, while debonding is a prerequisite for high toughness, the properties of the composite are not otherwise limited by the extent of debonding. The basic fracture requirement for the interface is thus;

$$\mathcal{G}_i/\mathcal{G}_f \lesssim 1/4$$

at $\psi = \pi/4$ when $\Sigma = 1$. Trends in this prerequisite with Σ remain to be characterized. Subject to this requirement, the sliding resistance of the debonded interface is the most important interface property, as elaborated in subsequent sections.

One additional issue concerns thermal debonding in composites subject to residual radial tension, as governed by the inequality,[12] $q \gtrsim \sqrt{\pi E \mathcal{G}_m/2R}$. When this inequality is satisfied, the incidence of thermal debonding is influenced by the interface flaw statistics, such that the debond probability increases as q becomes large. The thermal debonds typically extend about 2/3 around the circumference (see Fig. 10) before arresting.[17] When thermal debonds exist, fiber failure at the crack front is inhibited and the requirements on $\mathcal{G}_i$ needed for good composite toughness are less stringent than those expressed above.

There is no direct experimental validation of the preceding hypothesis for ceramic matrix composites. However, various observations of crack interactions with fibers and whiskers are supportive of the general features.[17,21] In particular, experiments on LAS/SiC composites reveal that as-processed materials with a

C interlayer debond readily and demonstrate extensive pull-out (Fig. 10a), whereas composites heat treated in air to create a continuous SiO_2 layer between the matrix and fiber exhibit matrix crack extension through the fiber without debonding (Fig. 10b). Furthermore, composites with a thin interface layer of SiO_2 having a partial circumferential gap exhibit intermediate pull-out characteristics (Fig. 10c). The associated constituent properties are summarized in Table I. Based on these properties, the preceding arguments would indicate that crack front debonding should not occur when a complete SiO_2 layer exists at the interface; whereas, appreciable crack front debonding should obtain when the C layer is present, in complete accordance with the observations.[17,21] The composites with only a partial SiO_2 interface layer are also interesting. For these materials, $\mathcal{G}_i$ is related to that fraction of the circumference that bonds the fiber to the matrix: typically 1/3 (Fig. 10c). Reference to Table I and to the initial debonding requirement (Eqn. 7) would thus indicate that debonding, while marginal, is certainly possible.

A second pair of examples concerns SiC whiskers in Al_2O_3 and Si_3N_4 matrices with an amorphous silicate interphase.[22] For these materials, the properties indicated in Table II indicate that crack front debonding conditions are marginally satisfied, consistent with the variability in debonding evident from toughness data.

5. PULL-OUT

An integral aspect of the analysis of composite fracture involves consideration of fiber failure and of subsequent pull-out. As noted above, fiber failure can usually be described using concepts of weakest link statistics based on the fiber strength parameters S_o and m,[20] in accordance with the frequency distribution,

$$\int g(S)dS = (S/S_o)^m \qquad (13)$$

The locations of fiber failure that govern the pull-out distributions can, in principle, be determined from the stresses on the fibers ahead of the matrix crack and in the crack wake. The former analysis has not been attempted, partly because the problem is complex and partly because of a perception that fiber failures close to the crack plane that cause pull-out are most likely to occur in the crack wake, following the debond extension process. Indeed, such behavior has been observed in glass reinforced plastics.[23] However, there is no direct evidence that fiber failure ahead of the matrix crack can be neglected in ceramic matrix composites.

While it is important to be aware of the above uncertainties, it is nevertheless insightful to fully analyze the wake failure phenomenon. Comparisons with experimental fiber pull-out data then allow assessment of the hypothesis. The fiber failure analysis commences with the basic weakest link description of failure. Then, by incorporating an axial fiber stress distribution, the fiber failure locations can be derived.[20] Such analysis has been performed for composites with negligible residual stress and having debonded interfaces subject to a constant sliding stress τ. For this purpose, the fundamental probability density function is[20]

$$\phi(z,t) = \frac{2\pi R m}{S_o^m}(t - 2z\tau/R)^{m-1}\exp\left[-(t/T)^{m+1}\right] \qquad (14)$$

where

$$T = \left[\frac{S_o^m \tau(m+1)}{2\pi R^2}\right]^{\frac{1}{(m+1)}}$$

and z is the distance from the crack plane. Then, the cumulative probability that the pull-out length will be $\leq h$ is ($h < t\,R/2\tau$),[21]

$$\Phi(h) = 2\int_o^h \int_o^{\bar{}} \phi(z,t)\,dzdt \qquad (15)$$

Trends in cumulative probability are plotted on Fig. 11, indicating that the pull-out lengths tend to increase as m decreases. The effects of residual strain on Φ (h) are expected to be substantial. Preliminary estimates suggest that the pull-out length usually decreases as the residual strain ε increases, when the residual stress at the interface is compressive. However, specific trends are sensitive to m, as well as to the friction coefficient μ.

Experimental results concerning trends in the pull-out distribution with interface properties[21] have been obtained for heat treated LAS/SiC composites, having the features described in the preceding section (Fig. 10). The results reveal that as the gap caused by C removed is filled with SiO_2, the pull-out distribution gradually changes (Fig. 12). In particular, the median length decreases and that proportion of fibers that actually pull out exhibit length distributions consistent with those predicted by the above weakest link fiber failure analysis (Fig. 12) such that the interface τ increases by about an order of magnitude when a partial SiO_2 layer replaces C. This change in τ causes a dramatic change in the mechanical properties of the composite, as elaborated below.

III TENSILE PROPERTIES: MODE I FAILURE

1. AXIAL STRESS–STRAIN BEHAVIOR

The axial tensile properties of ceramic matrix composites are strongly influenced by the relative debond resistance $\mathcal{G}_i(\psi)/\mathcal{G}_f$, by the friction coefficient along the debonded interface μ and by the residual strain, ε, as intimated in the preceding section. When the interface is in residual tension and when $\mathcal{G}_i/\mathcal{G}_f$ and μ are both small, as exemplified by C interlayers between fiber and matrix, experience[21,24] has indicated that the tensile stress/strain behavior illustrated in Fig. 13a obtains. Three features of this curve are important: matrix cracking at a stress σ_o, fiber bundle failure at σ_u and the pull-out stress. Increases in either $\mathcal{G}_i/\mathcal{G}_f$ or μ cause the stress–strain curve to become linear[21] (Fig. 13b). Furthermore, the ultimate strength then coincides with the propagation of a single dominant crack (albeit, sometimes with a desirable "tail" caused by delamination, as discussed in Section 4). Composites having this macroscopic characteristic exhibit properties governed by a fracture resistance curve. The individual properties within each of these two regimes are discussed below, as well as criteria that dictate the transition between regimes.

i) Matrix Cracking

The stress σ_o at which matrix cracking occurs has been the most extensively studied behavior in ceramic matrix composites.[15,24-26] For composites in which q is tensile and the interface properties can be effectively represented by an unique sliding stress, τ, the matrix cracking stress is given by;[15]

$$\frac{\sigma_o}{E} = \left(\frac{6 f^2 E' \tau \mathcal{G}_M}{(1-f) E (E^M)^2 R}\right)^{\frac{1}{3}} - \frac{p}{E^M} \qquad (16)$$

This result is independent of the matrix crack length because the crack is bridged by fibers. Experiments conducted on a number of ceramic matrix composites have validated Eqn. (16). When the interface is subject to residual compression, τ depends on the applied stress and the solution for σ_o is more complex. However, to first order, τ may be simply replaced by μq. At σ_o, multiple matrix cracking is expected[25] and observed[26] with a saturation crack spacing D in the range;

$$\sigma_o R/2f\tau < D < \sigma_o R/f\tau \qquad (17)$$

Experimental observations[24] have again confirmed this feature of matrix cracking.

The most crucial aspects of the above interpretation of steady-state cracking and of behavior prediction concern determination of τ and q for actual composite system. Both are difficult to measure. Two basic approaches have been used to measure the sliding resistance τ : indentation[27,28] and crack opening hysteresis.[24] Both approaches are readily applicable when $\mathcal{G}_i$ and τ are small. The former method is most insightful when used with a nanoindenter system, whereupon τ can be obtained on single fibers either from a push through force on thin sections or from the hysteresis in the loading/unloading cycle on thick sections (Fig. 14a). However, this method has the obvious disadvantage that the fiber is in axial compression such that the debond interface is also compressed during the test, with attendant changes in τ. Matrix cracking followed by measurement of the crack opening hysteresis (Fig. 14b) is more desirable, when feasible, because the fibers are subject to axial tensile loading. However, when appreciable fiber failure accompanies matrix

cracking, erroneous results also obtain for this method. Both approaches give about the same value of τ for composites having the following characteristics: tensile residual strain exists at the interface,[24] $\mathcal{G}_i/\mathcal{G}_f$ is small and τ is small (< 10MPa). Otherwise, both approaches are problematic. Consequently, other approaches applicable to composites having larger τ are being investigated. One of these is discussed in the following section.

ii) **The Ultimate Strength**

Following multiple matrix cracking, the fibers are subject to an oscillating stress field with maximum equal to σ_∞/f between the crack surfaces where σ_∞ is the applied stress. The probability of fiber failure within such a stress field subject to weakest link statistics can be readily derived.[29] However, derivation of a load maximum requires that the stress redistribution caused by the fractured fibers be modelled. Such an analysis has not been attempted. Nevertheless, a lower bound for the load can be derived by simply allowing failed fibers to have no load bearing ability. Then, a modified bundle failure analysis allows the ultimate strength to be;[34]

$$\sigma_u = f\hat{S} \exp\left[-\frac{\left[1-(1-\tau D/R\hat{S})^{m+1}\right]}{(m+1)\left[1-(1-\tau D/R\hat{S})^{m}\right]} \right] \qquad (18)$$

where S_o and m are the statistical parameters that represent the fiber strength distribution and

$$(R\hat{S}/\tau D)^{m+1} = (1/2\pi RL)(RS_o/\tau D)^m\left[1-(1-\tau D/R\hat{S})^{m}\right]^{-1} \qquad (19)$$

with L being the gauge length. In the one composite system for which analysis of the ultimate strength has been performed (LAS/SiC),[21] surprisingly Eqn. (18) agrees quite well with measured values.

The ultimate strength anticipated from the above logic is expected to be influenced by the residual stress. Specifically, in systems for which the fiber is subject to residual compression, the axial compression should suppress fiber failure and elevate the ultimate strength to a level in excess of that predicted by Eqn. (18). This effect may be estimated by regarding the matrix as clamping onto the fiber and thus, simply superposing the residual stress onto $\hat{S}$.

iii) **Resistance Curves**

When mode I failure is dominated by propagation of a single dominant matrix crack, accompanied by fiber failure and pull-out, the mechanical properties are characterized by a resistance curve. Analysis of this phenomenon utilizes the distribution of fiber failure sites determined in the pull-out analysis (Fig. 11). From such analysis, the mean failure length of all fibers that fail at stress t acting on the fiber between the crack surfaces is first evaluated.[20] Then, by taking into account the reduced stress caused by fiber failure and knowing the associated crack opening, u, the total stress on the fibers between the crack at a fixed crack opening may be determined,[20] as plotted on Fig. 15. Several features of the t (u) curve are notable. The initial, rising position is dominated by intact fibers, the peak is dominated by multiple fiber failures, analogous to bundle failure, and the tail is governed by pull-out. The role of the shape parameter, m, on these features is particularly interesting. As m decreases, corresponding to a broader distribution of fiber strengths, more fibers fail further from the matrix crack (Fig. 11) causing the extent of pull-out to substantially increase.

The trends in t(u) directly associate with the two most relevant features of the fracture resistance curves: the asymptotic toughness and the slope (or tearing modulus), respectively. The asymptotic toughening can be simply derived from the J integral result,

$$\Delta \mathcal{G}_{ss} = 2f \int_0^{\bar{} } t(u)du \qquad (20)$$

The expressions that govern the trends in $\Delta \mathcal{G}_{ss}$ with material properties are unwieldy in form.[20] However, inspection reveals that $\Delta \mathcal{G}_{ss}$ always increases as the scale parameter S_0 increases, thereby establishing that high fiber strengths are invariably desirable. However, the dependence on τ and R is ambivalent. The essential details are highlighted by considering separately the bridging and pull-out contributions to the toughness integral. The bridging component

$$\Delta \mathcal{G}_b = 4fTU/(m+1) \qquad (21)$$

where $U = T^2R/4E^f\tau(1+\xi)$ is proportional to $[R^{m-5}/\tau^{m-2}]^{1/(m-1)}$. A notable feature is the inversion in the trend with that τ occurs at $m = 2$, and with R at $m = 5$. The corresponding pull-out contribution can be examined by recognizing that the toughening has the form

$$\Delta \mathcal{G}_b \sim (h)^2(\tau/R) \qquad (22)$$

which, with Eqn. (15) indicates a toughness proportional to $\left[R^{m-3}S_o^{2m}/\tau^{m-1}\right]^{\frac{1}{(m+1)}}$. The toughness thus increases with increasing R when $m > 5$, and decreases when $m < 3$. Conversely, it increases with increasing τ when m is very small (≤ 1), and decreases

when $m > 2$. These limits arise because of the competing importance of the contribution to toughness from the intact bridging fibers and the failed fibers that experience pull-out. Knowledge of the magnitude of the statistical shape parameter, m, for the fibers *within* the composite is therefore a prerequisite to optimizing the shear properties of the interface for high toughness.

The slope of the resistance curve has not yet been evaluated, because numerical methods are needed to determine the upper limit of Eqn. (20), as dictated by the crack opening at the end of the bridging zone. Yet, this shape has a major influence upon the ultimate strength of the composite. Further research concerning this phenomenon is a major priority.

iv) Property Transition

Non-linear macroscopic mechanical behavior in tension is most desirable for structural purposes and thus, analysis of the transition between this regime and the linear regime is important. A useful preamble involves comparison of the basic trends in the steady-state matrix cracking stress, σ_0 (Eqn. 16), and in the asymptotic fracture resistance, $\Delta \mathcal{G}_{ss}$ (Eqn. 20). At the simplest level,* these trends are

$$\sigma_o \sim (\tau/R)^{1/3}$$
$$\Delta \mathcal{G}_{ss} \sim RS_o^2/\tau \qquad (23)$$

Most significantly, σ_0 increases but $\Delta \mathcal{G}_{ss}$ decreases as τ increases. These opposing trends with τ suggest the existence of an optimum τ that permits good matrix cracking resistance while still allowing high toughness.

*These trends apply except at small m.

More specifically, a property transition is expected when the matrix cracking stress attains the stress needed for fiber bundle failure. One bound on the property transition can be obtained by simply allowing σ_o to exceed the ultimate strength.[21,31] Then, the parameter B which governs the transition when τ is small is;

$$B = \tau E \mathcal{G}_M / S_o^3 R \tag{24}$$

Specifically, when B exceeds a critical value, linear behavior initiates. Experiments on heat treated LAS/SiC composites[21] have examined the conditions associated with this transition (Fig. 16).

v) Residual Stress

Large mismatches in thermal expansion between fiber and matrix are clearly undesirable. In particular, relatively large matrix expansions, $\alpha^m/\alpha^f >> 1$, cause premature matrix cracking (Eqn. 16). Such behavior is not necessarily structurally detrimental, but concerns regarding thermal fatigue, the ingress of environmental fluids, etc. have discouraged the development of materials having these characteristics. Conversely, very small matrix expansions, $\alpha^f/\alpha^m >> 1$, thermally debond the fiber from the matrix. When sufficiently extensive, such debonding results in axial separations that negate the influence of the fibers. Consequently, values of α^f/α^m close to unity are required. Indeed, mode I axial properties subject to an interface that easily debonds and slides freely along the debond involve an optimum residual stress, with a maximum matrix cracking stress, when ε is positive, given by,[15]

$$\sigma_o/E = (2/3)\left[f\mu\mathcal{G}_M/\lambda_2 E_M R\right]^{\frac{1}{2}} \tag{25}$$

where

$$\lambda_1 = \frac{1-(1-E/E_f)(1-\nu_f)/2+(1-f)(\nu_m-\nu_f)/2-(E/E_f)\left[\nu_f+(\nu_m-\nu_f)fE_f/E\right]^2}{(1-\nu_m)\Delta},$$

$$\lambda_2 = \frac{\left[1-(1-E/E_f)/2\right](1+\nu_f)+(1+f)(\nu_m-\nu_f)/2}{\Delta},$$

and

$$\Delta = 1+\nu_f+(\nu_m-\nu_f)fE_f/E$$

When $\alpha_f/\alpha_m >> 1$, such that ε is negative, asperities on the debond surface may provide a discrete sliding stress, τ, that depends on such features as the asperity amplitude. For such cases, the optimum residual strain has not been determined. It is noted, however, that good properties have been demonstrated for LAS/SiC composites having an expansion mismatch, $\Delta\alpha \sim 3\times10^{-6}\,C^{-1}$.

The above remarks concerning residual strains are qualified by debonding requirements. While the condition $\mathcal{G}_i/\mathcal{G}_f < 1/4$ ($\Sigma = 1$) is an adequate prerequisite for debond initiation of the matrix crack front, it is not clear at this stage whether smaller values are needed when ε is positive, in order to ensure that debonding occurs to a sufficient extent that the pull-out distribution is not diminished by fiber failure from the debond.

The fracture resistance is also influenced by the residual stress. However, the sign and magnitude of the change in toughness induced by residual stress depends on the mechanisms of interface sliding and fiber failure, as summarized in Table III.

Subject to adequate debonding, the salient result for ceramics reinforced with brittle fibers is that $\Delta \mathcal{G}_{ss}$ is unaffected when ε is negative and the interface is characterized by an unique τ, whereas $\Delta \mathcal{G}_{ss}$ usually decreases with increase in ε when ε is positive because the pull-out lengths decrease, as apparent when τ in Fig. 11 is equated to μq.

Residual stresses in composites are difficult to measure. Even when the composite is fully elastic, such that no interface debonding or sliding occur on cooling, the residual stress at the surfaces are still complex. Consequently, methods such as X-ray diffraction that probe thin surface layers are difficult to interpret. Neutron diffraction, which typically averages over a much larger volume of material, is usually more satisfactory. Measurement difficulties are exacerbated when debonding and sliding occur on cooling. These processes initiate preferentially at the surface and spread into the body along the interface, thereby alleviating the residual stress over the debond/slip length. For small τ and $\mathcal{G}_i$, these lengths are large (many multiples of the fiber diameter).[24] Consequently, a valid measure of the residual stress can only be obtained using processes that penetrate well into the material. One independent approach for measuring q that has merit in some cases involves use of the same crack opening measurements described by Fig. 14b. Specifically, the residual axial stress in the matrix is related directly to the stress at which crack closure occurs.[24] The method is, however, restricted to materials for which matrix cracking is not accompanied by extensive fiber failure.

2. TRANSVERSE FAILURE

The transverse strength of high toughness composites are generally very low. There have been no systematic studies of this property. However, experimental studies on composite laminates[32] indicate that the transverse cracks typically propagate along the interface layer and through the matrix between neighboring

fibers. Furthermore, because the interfaces have sufficiently small $\mathcal{G}_{ic}$ to allow debonding, overall failure is preceded by interface failure. This process is assumed to occur at a critical stress, σ_c, which can be determined in a manner analogous to that for the steady-state cracking of thin films,[33] to give,

$$\sigma^c = \sqrt{2E\mathcal{G}_i/\pi R} - q \tag{26}$$

In some cases, q is sufficiently large that $\sigma^c < 0$ and the interfaces debond upon cooling (Fig. 10). Overall failure involves the coalescence of interface cracks. This occurs at another critical stress, which is related to the solution for an array of parallel cracks.

IV MIXED MODE FAILURE

1. MODE II FAILURE MECHANISMS

Flexural tests performed on uniaxial composites reveal that a shear damage mechanism exists (Fig. 11)[24,32,34] and that such damage often initiates at quite low shear stresses, e.g., 20MPa in LAS/SiC. The damage consists of en echelon matrix microcracks inclined at about $\pi/4$ to the fiber axis (Fig. 17). With further loading, the microcracks coalesce, causing matrix material to be ejected and resulting in the formation of a discrete mode II crack. The crack is defined by the planar zone of ejected matrix. The crack also has a microcrack damage zone similar to that present upon crack initiation.

The microcracks that govern mode II failure are presumably caused by stress concentrations in the matrix and form normal to the local principal tensile stress,

but then deflect parallel to the mode II plane and coalesce. An adequate model that incorporates the above features has not been developed. Consequently, the underlying phenomena are briefly noted without elaboration. The stress concentrations in the matrix have magnitude governed by the elastic properties, the fiber spacing and the interface strength. The growth and coalescence of the microcracks scales with the matrix toughness $\mathcal{G}_{mc}$. The shear strength seemingly decreases as the mode I toughness increases.

2. DELAMINATION CRACKING

Delamination is a common damage mode in the presence of notches[32] (Fig. 11). Delamination cracks nucleate near the notch base and extend stably (Fig. 18). Analysis of such data is based on the solutions used for mixed mode interface cracking in beams,[9] modified to take account of the elastic anisotropy. The fracture resistance is found to increase with crack extension and, because of the large phase angle, the fracture mechanism is essentially identical to that noted for mode II failure, involving matrix microcracking and spalling. The existence of a resistance curve is attributed to intact fibers within the crack that resist the displacement of the crack surfaces and thus, shield the crack tip in a manner analogous to fiber bridging in mode I. However, explicit analysis has yet to be conducted.

V MICROSTRUCTURE DESIGN

Many of the microstructural parameters that control the overall mechanical properties of ceramic matrix composites are now known and validated, as elaborated

in the preceding sections. Consequently, various general remarks about microstructure design can be made However, important aspects of damage and failure are incompletely understood because there have been few organized studies of failure in mode II, mixed mode and transverse mode I. The remarks made in this section thus refer primarily to axial mode I behavior with no special regard to attendant problems in other loading modes.

The basic microstructural parameters that govern mode I failure are the relative fiber/matrix interface debond toughness, $\mathcal{G}_i/\mathcal{G}_f$, the residual strain, ε, the friction coefficient of the debonded interface, μ, the statistical parameters that characterizes the fiber strength, So and m, the matrix toughness, $\mathcal{G}_m$, and the fiber volume fracture f. The prerequisite for high toughness is that $\mathcal{G}_i/\mathcal{G}_f \lesssim 1/4\,(\Sigma = 1)$. Subject to this requirement, the residual strain must be small ($\Delta\alpha \lesssim 4 \times 10^{-6}\,C^{-1}$) and negative such that the interface is in tension. Furthermore, the friction coefficient along the debonded interface should be small ($\mu \lesssim 0.1$). The ideal fiber properties are those that encourage large pull-out lengths, as manifest in an optimum combination of a high median strength (layer S_o) and large variability (small m).

The above conditions can be satisfied, in principal, by creating interphases between the fiber and matrix, either by fiber coating or, in-situ, by segregation. The most common approach is the use of a dual coating: the inner coating satisfies the above debonding and sliding requirements, while the outer coating provides protection against the matrix during processing. However, the principal challenge is to identify an inner coating that has the requisite mechanical properties while also being thermodynamically stable in air at elevated temperatures. Most existing materials have either C or BN as the debond layer. However, both materials are prone to degradation in air at elevated temperatures. More stable alternatives have been proposed (e.g., Nb, Mo, Pt, NbAl) but have not been evaluated.

TABLE I

Constituent Properties of LAS/Nicalon Composites

	E(GPa)	$\mathcal{G}_c$ (Jm^{-2})	α (K^{-1})
Fiber (Nicalon)	200	4 – 8≠	4×10^{-6}
Matrix (LAS)	85	40	1×10^{-6}
Interface			
Amorphous C	——	< 1 *	——
Amorphous SiO_2	80	8	1×10^{-6}

≠ Determined from fracture mirror radii

* Determined by indentation: takes into account initial thermal debonding (Fig. 10)

TABLE II

Constituent Properties of Whisker-Reinforced Ceramics

	E(GPa)	$\mathcal{G}_c$ (Jm^{-2})	α (K^{-1})
Al_2O_3	400	20 – 30	7×10^{-6}
Si_3N_4	300	60 – 80	3×10^{-6}
SiC	400	15 – 20	4×10^{-6}
Amorphous interface	70	4 – 8	——

TABLE III

Effect of Residual Stress on Toughness

STRESS/DISPLACEMENT LAW		RUPTURE CONDITION	RESIDUAL STRESS IN FIBER	
			COMPRESSION	TENSION
Linear		Stress	Decrease	Decrease
		Displacement	Increase	Decrease
Frictional With Pull-Out	Surface Roughness	Stress	--------	Negligible
	Coulomb Friction	Stress	Decrease	--------

REFERENCES

[1] A. G. Evans and R. M. Cannon, Acta Met. 34, (1986) 761.

[2] J. W. Hutchinson, Acta Met, 35, (1987) 1605.

[3] M. Rühle, A. G. Evans, R. M. McMeeking and J. W. Hutchinson, Acta Met. 35, (1987) 2701.

[4] A. G. Evans and K. T. Faber, J. Am. Ceram. Soc. 67, (1984) 255.

[5] B. Budiansky, J. W. Hutchinson and J. Lambropolous, Intl. Jnl. Solids and Structures, 19, (1983) 337.

[6] J. W. Hutchinson, Non-Linear Fracture Mechanics, Tech. Univ. Denmark (1979).

[7] J. R. Rice, Fracture, Vol. 11 (ed., H. Liebowitz), Academic Press, NY (1968) p. 191.

[8] J. R. Rice, J. Appl. Mech., in press.

[9] P. G. Charalambides, R. M. McMeeking and A. G. Evans, J. Appl. Mech., in press.

[10] J. Dundurs, Mathematical Theory of Dislocations, ASME, NY (1969) p. 70.

[11] A. G. Evans and J. W. Hutchinson, Acta Met., in press.

[12] P. G. Charalambides and A. G. Evans, Advanced Ceramic Materials, in press.

[13] L. S. Sigl and A. G. Evans, to be published.

[14] Z. Suo and J. W. Hutchinson, Harvard University Report MECH, 118 (1988), Intl. J. Frac., in press.

[15] B. Budiansky, J. W. Hutchinson and A. G. Evans, J. Mech. Phys. Solids, 34, (1986) 167.

[16] E. Bischoff, O. Sbaizero, M. Rühle and A. G. Evans, Advanced Ceramic Materials, in press.

[17] M. Y. He and J. W. Hutchinson, Harvard University Report MECH, 113 (1988), J. Appl. Mech., in press.

[18] H. C. Cao and A. G. Evans, to be published.

[19] P. G. Charalambides, H. C. Cao, J. Lund and A. G. Evans, to be published.

[20] M. D. Thouless and A. G. Evans, Acta Met. 36, (1988) 517.

[21] M. D. Thouless, O. Sbaizero, L. S. Sigl and A. G. Evans, Advanced Ceramic Materials, in press.

[22] M. Rühle, B. J. Dalgleish and A. G. Evans, Scripta Met. 21, (1987) 681.

[23] J. K. Wells, Ph.D. dissertation, Cambridge Univ. (1982).

[24] D. B. Marshall and A. G. Evans, J. Am. Ceram. Soc. 68, (1985) 225.

[25] J. Aveston, G. A. Cooper and A. Kelly, The Properties of Fiber Composites, JPC Science Technology (1971) p. 15.

[26] D. B. Marshall, B. N. Cox and A. G. Evans, Acta Met. 33, (1985) 2013.

[27] D. B. Marshall and W. Oliver, J. Am. Ceram. Soc., 70, (1987) 542.

[28] T. Wiehs and W. D. Nix, MRS Symposium, Reno, NV, Spring 1988.

[29] D. Johnson Walls, M.S. Thesis, University of California, Berkeley (1986).

[30] D. B. Marshall and A. G. Evans, Materials Forum, in press.

[31] E. Y. Luh and A. G. Evans, J. Am. Ceram. Soc. 70, (1987) 466.

[32] O. Sbaizero and A. G. Evans, J. Am. Ceram. Soc. 69, (1986) 481.

[33] M. S. Hu and A. G. Evans, Acta Met., in press.

[34] A. G. Evans, Mat. Sci. Eng. 71, (1985) 3.

FIGURE CAPTIONS

Fig. 1. A schematic illustrating the failure modes observed in high toughness uniaxially reinforced ceramic matrix composites
- a) tension
- b) flexure

Fig. 2. A schematic illustrating the initial debonding of fibers at the crack front and fiber debonding in the crack wake

Fig. 3. Trends in critical strain energy release rate with the phase angle of loading: experimental results and predictions for a model involving contact at asperities on the crack surface

Fig. 4. The displacement of the surface of a crack at a bimaterial interface indicating the shear and opening displacement that accompany most external loading conditions

Fig. 5. Trends in energy release rate and phase angle for loads exerted on a fiber in the crack wake
- a) effects of debond length
- b) effects of applied stress t on steady-state, $\mathcal{G}_{ss}$,
- c) effects of applied stress t on phase angle ψ in steady-state regime
- d) effects of elastic modulus ratio on $\mathcal{G}_{ss}$ and ψ

Fig. 6. Energy release rates for a bimaterial beam tested in flexure
- a) trends with crack length for an elastically homogeneous system
- b) trends in steady-state energy release rate, $\mathcal{G}_{ss}$ with modulus and thickness ratios

Fig. 7. The energy release rate for crack front debonding

Fig. 8. Energy release rates for kinking of an interface crack into a fiber as a function of the phase angle of loading. Also shown is a typical critical energy release rate for an interface crack: a is one of the Dundurs' parameters (Eqn. 2). Kinking occurs when the critical values $\mathcal{G}_{fc}/\mathcal{G}_{ic}$ fall below the kinking level, $\mathcal{G}_i^k/\mathcal{G}_i$

Fig. 9. Some test specimens used to determine the fracture resistance of interfaces as a function of phase angle.

Fig. 10. Interfaces and pull-out in a composite consisting of LAS matrix and SiC (Nicalon) fibers
- a) As-processed indicating C interlayer and extensive pull-out
- b) heat treated in air for 16 hours at 800°C indicating a complete SiO_2 layer and no pull-out
- c) heat treated in air for 4 hours at 800°C indicating a partial SiO_2 layer–with gap–and variable pull-out

Fig. 11. The cumulative pull-out distribution for several values of the shape parameter, m

Fig. 12. Histograms indicating trends in pull-out length with heat-treatment

Fig. 13. Tensile stress–strain curves for ceramic matrix composites
- a) Small $\mathcal{G}_{ic}$, small μ
- b) Small $\mathcal{G}_{ic}$, large μ

Fig. 14.
- a) A load/unload cycle for nanoindentation of a fiber
- b) Crack opening hysteresis for a composite with intact fibers revealing the trends in both sliding resistance and residual stress

Fig. 15. Trends in non-dimensional crack openings stress t, with opening u for several values of the shape parameter, m

Fig. 16. Effects of heat treatment on the stress–strain behavior of LAS/SiC composites

Fig. 17. Matrix microcracks observed in the zone of shear failure

Fig. 18. Delamination cracking in notched flexure tests

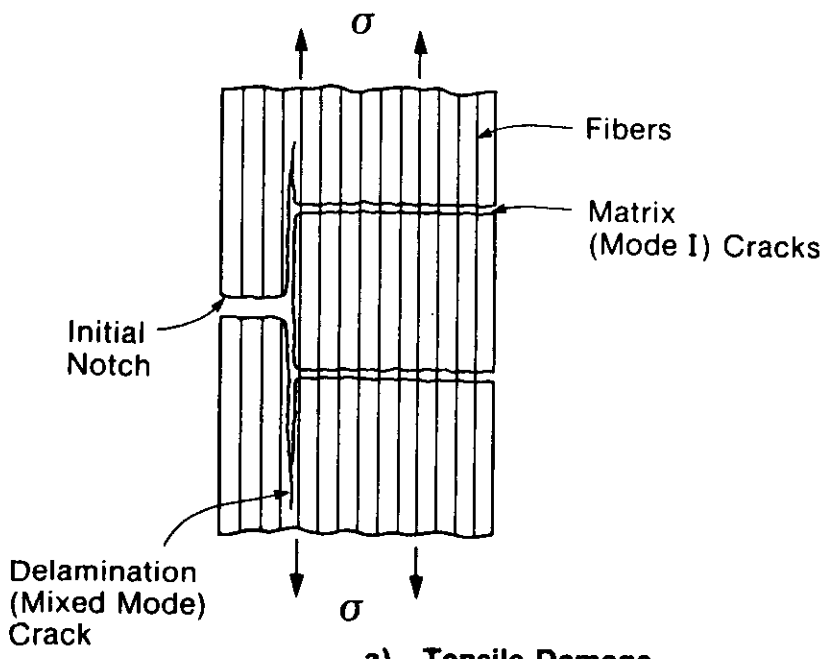

a) Tensile Damage

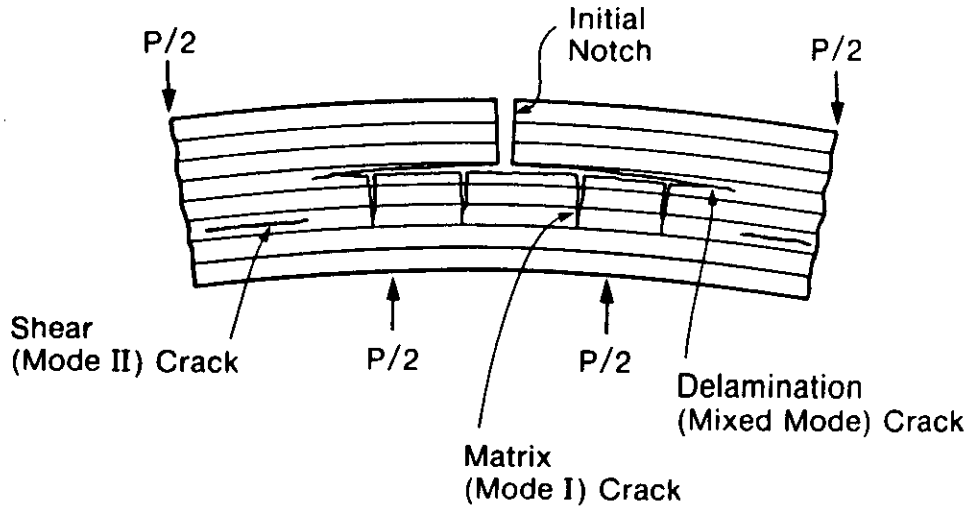

b) Flexural Damage

FIG. 1

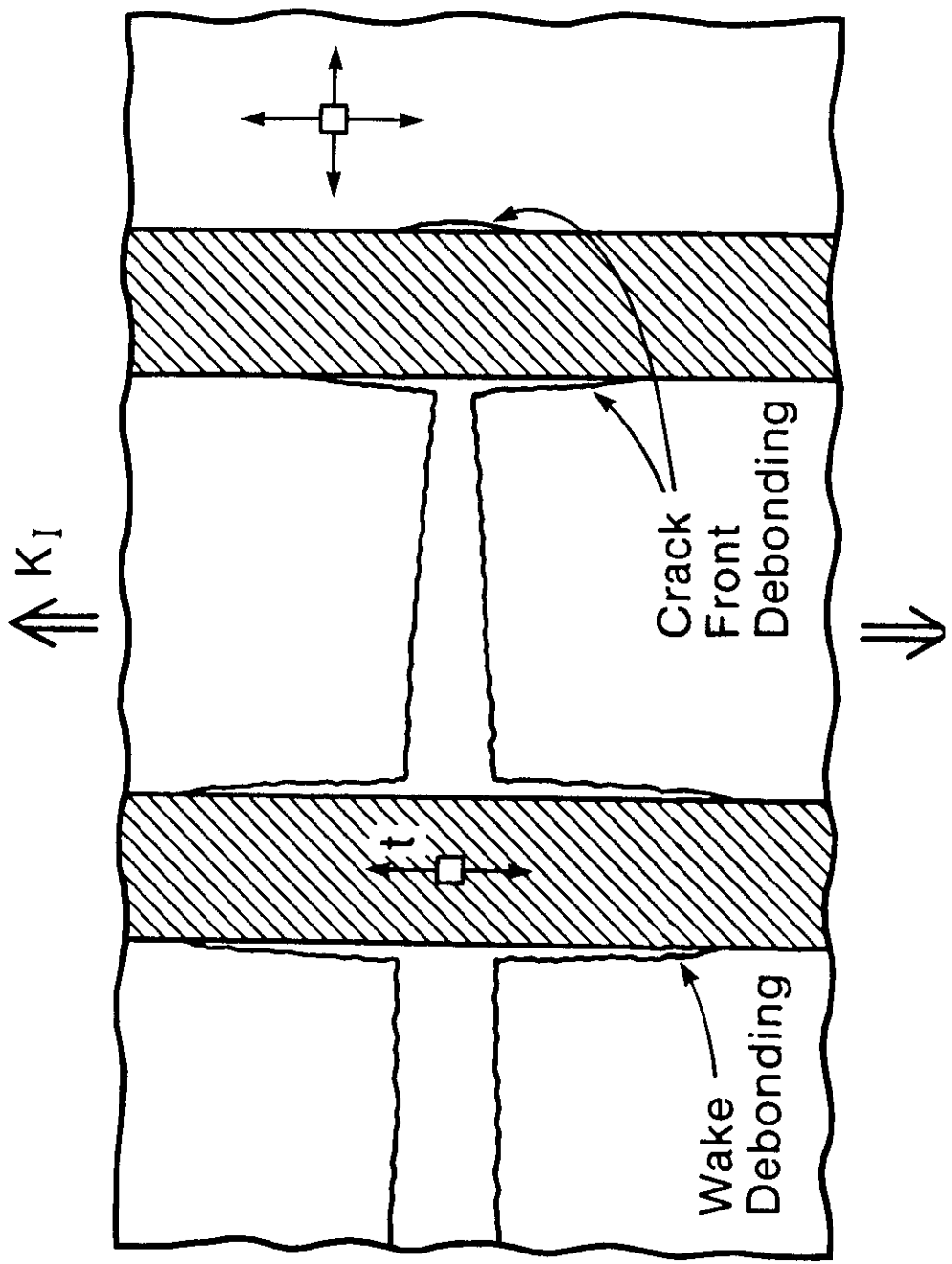
K_I
Crack Front Debonding
t
Wake Debonding

FIG. 2

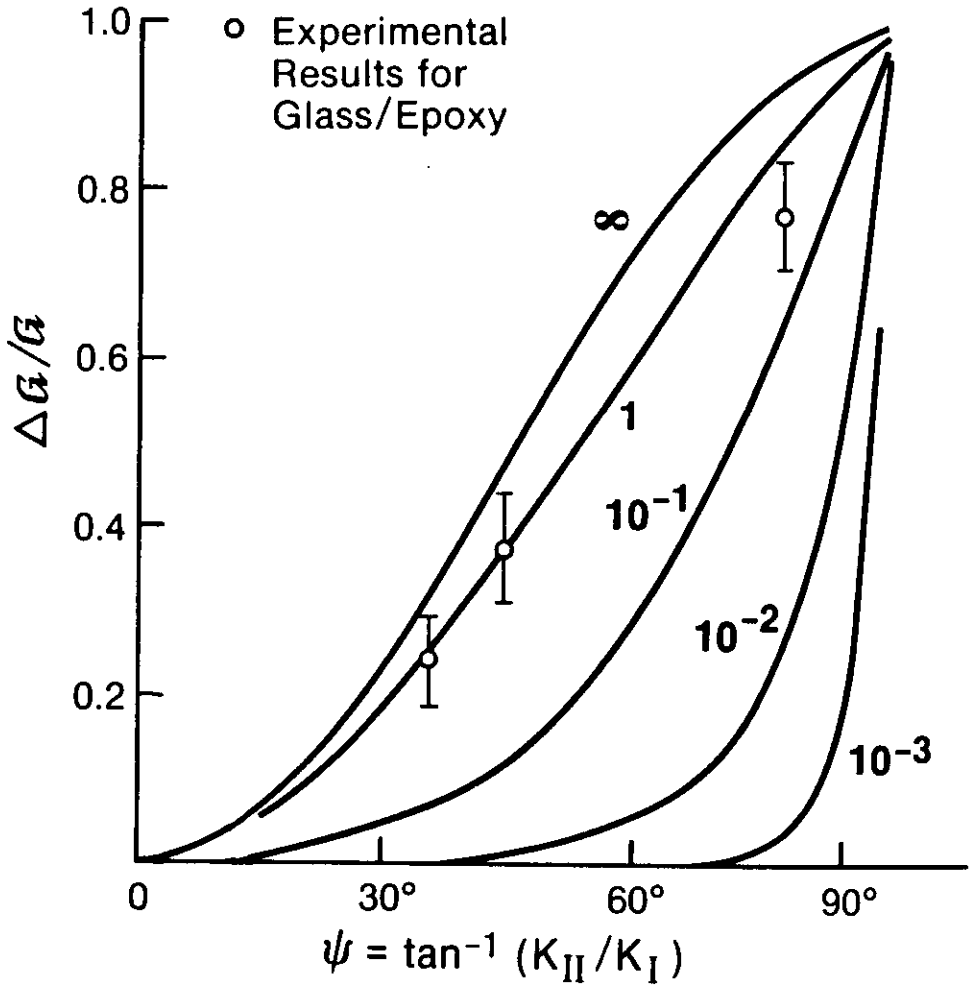
1.0
0.8
0.6
0.4
0.2
$\Delta G/G$
o Experimental Results for Glass/Epoxy
∞
1
10^{-1}
10^{-2}
10^{-3}
0
30°
60°
90°
$\psi = \tan^{-1}(K_{II}/K_I)$

FIG. 3

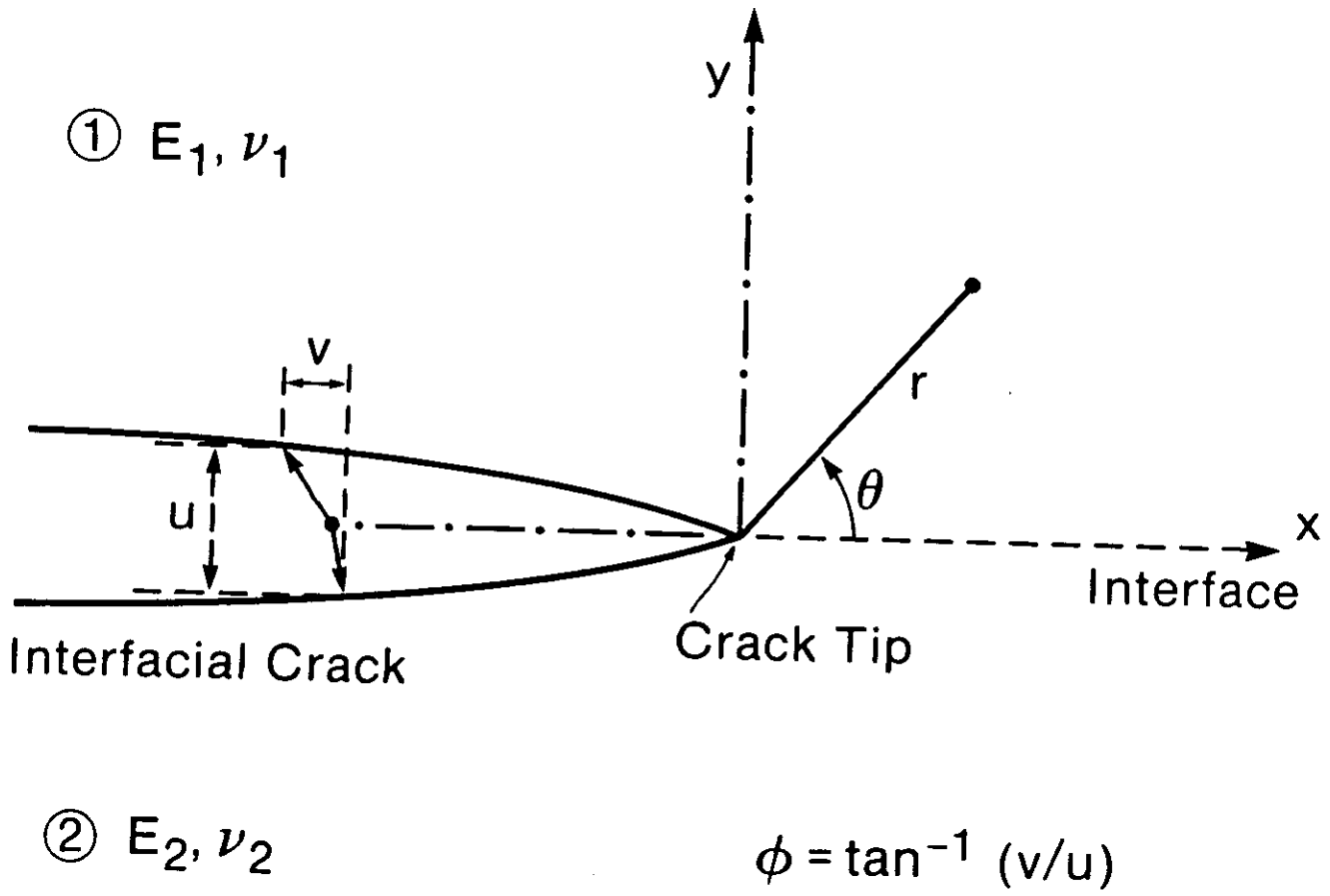

43

FIG. 4

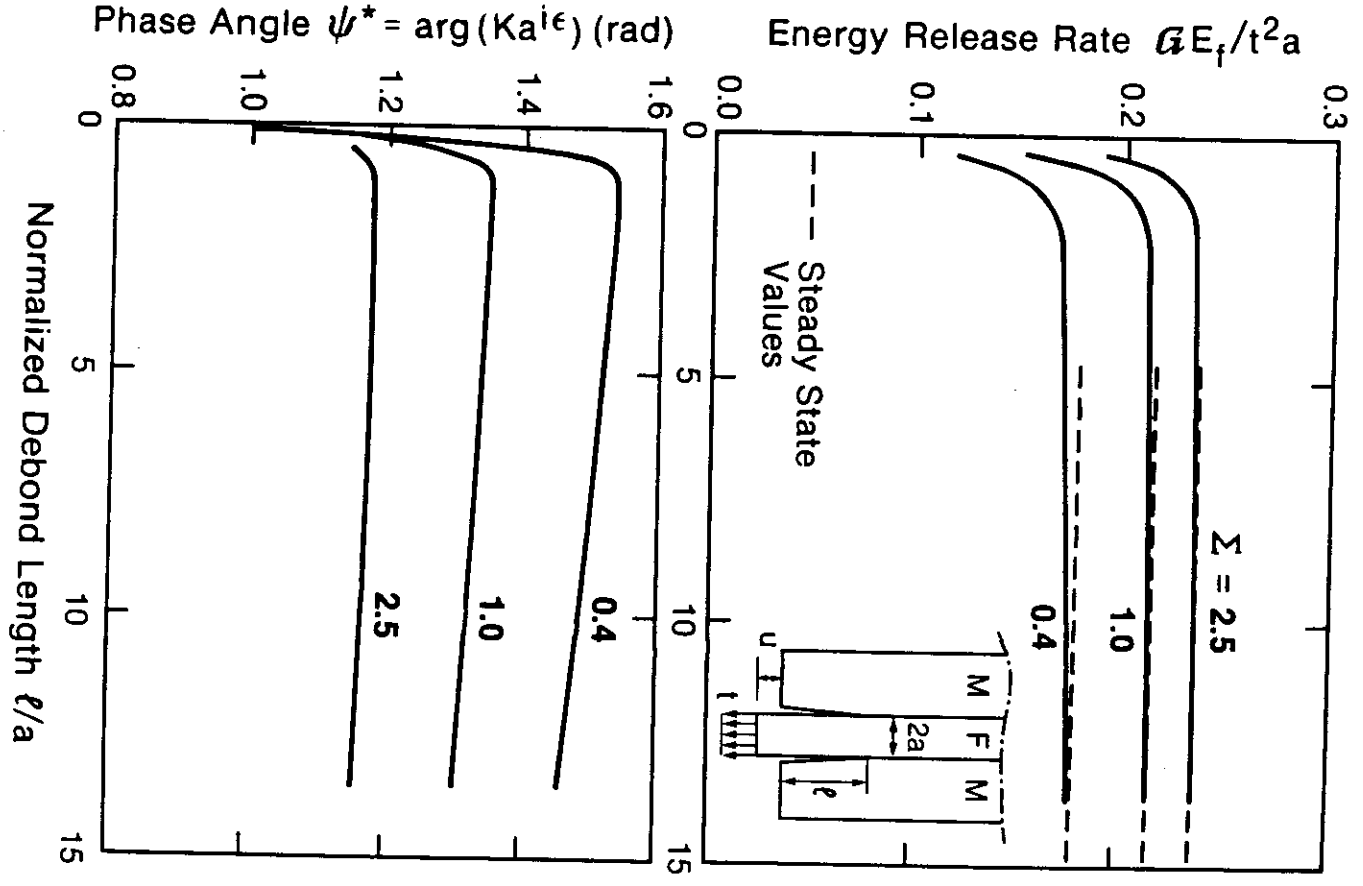

44

FIG. 5A

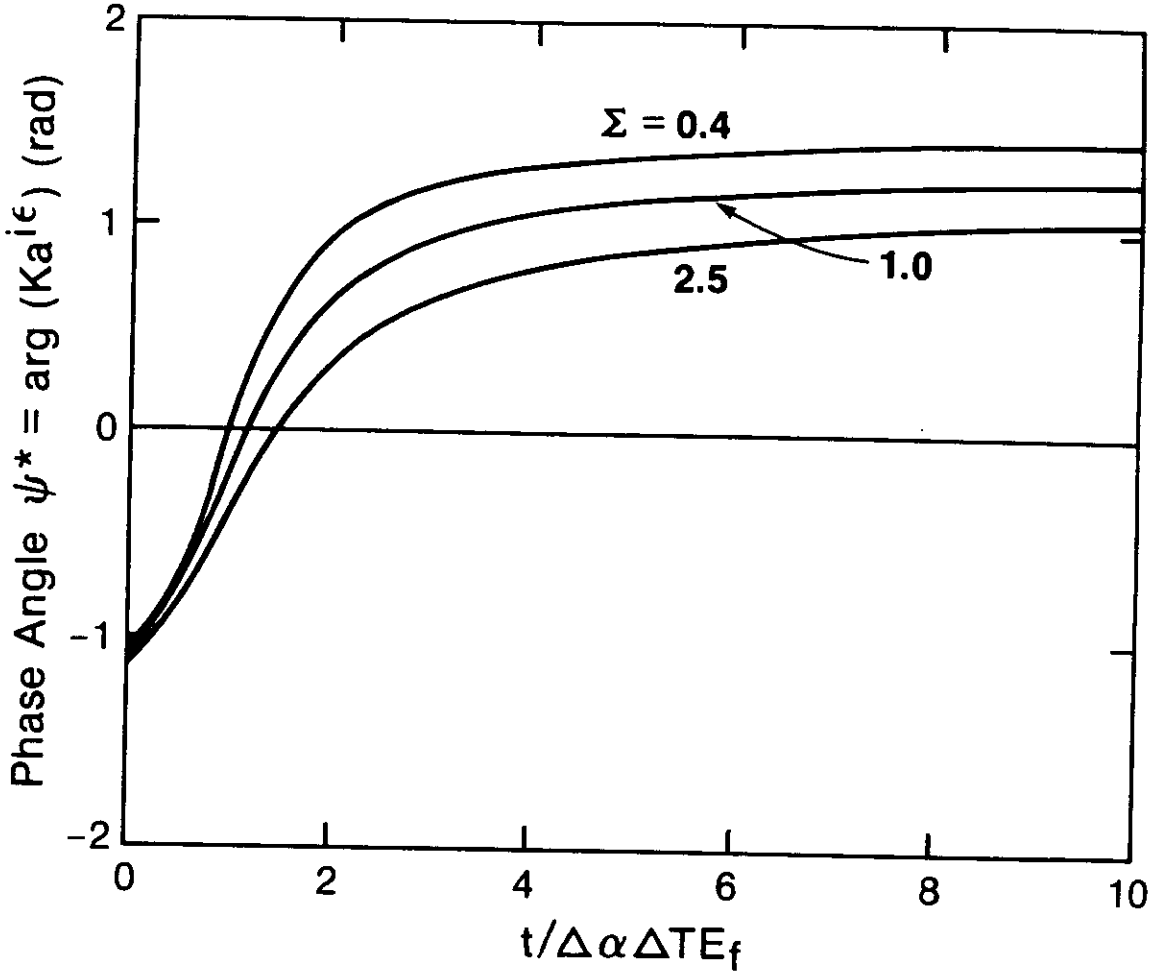
Phase Angle $\psi^* = \arg(Ka^{i\epsilon})$ (rad)
$t/\Delta\alpha\Delta T E_f$
Σ = 0.4
2.5
1.0
2
1
0
−1
−2
0
2
4
6
8
10

FIG. 5C

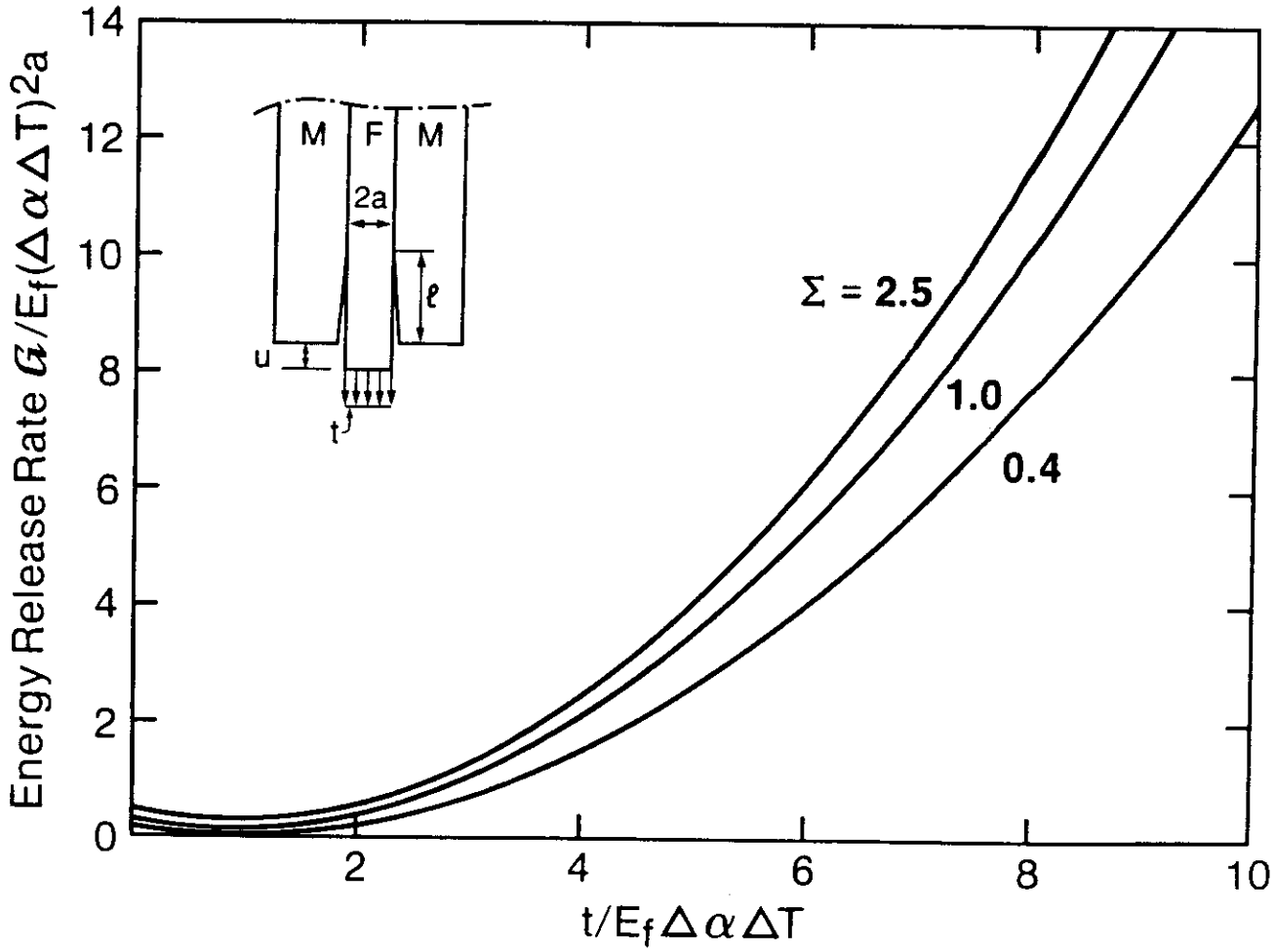
Energy Release Rate $G/E_f(\Delta\alpha\Delta T)^2 a$
$t/E_f\Delta\alpha\Delta T$
M
F
M
2a
ℓ
u
t
Σ = 2.5
1.0
0.4
14
12
10
8
6
4
2
0
2
4
6
8
10

FIG. 5B

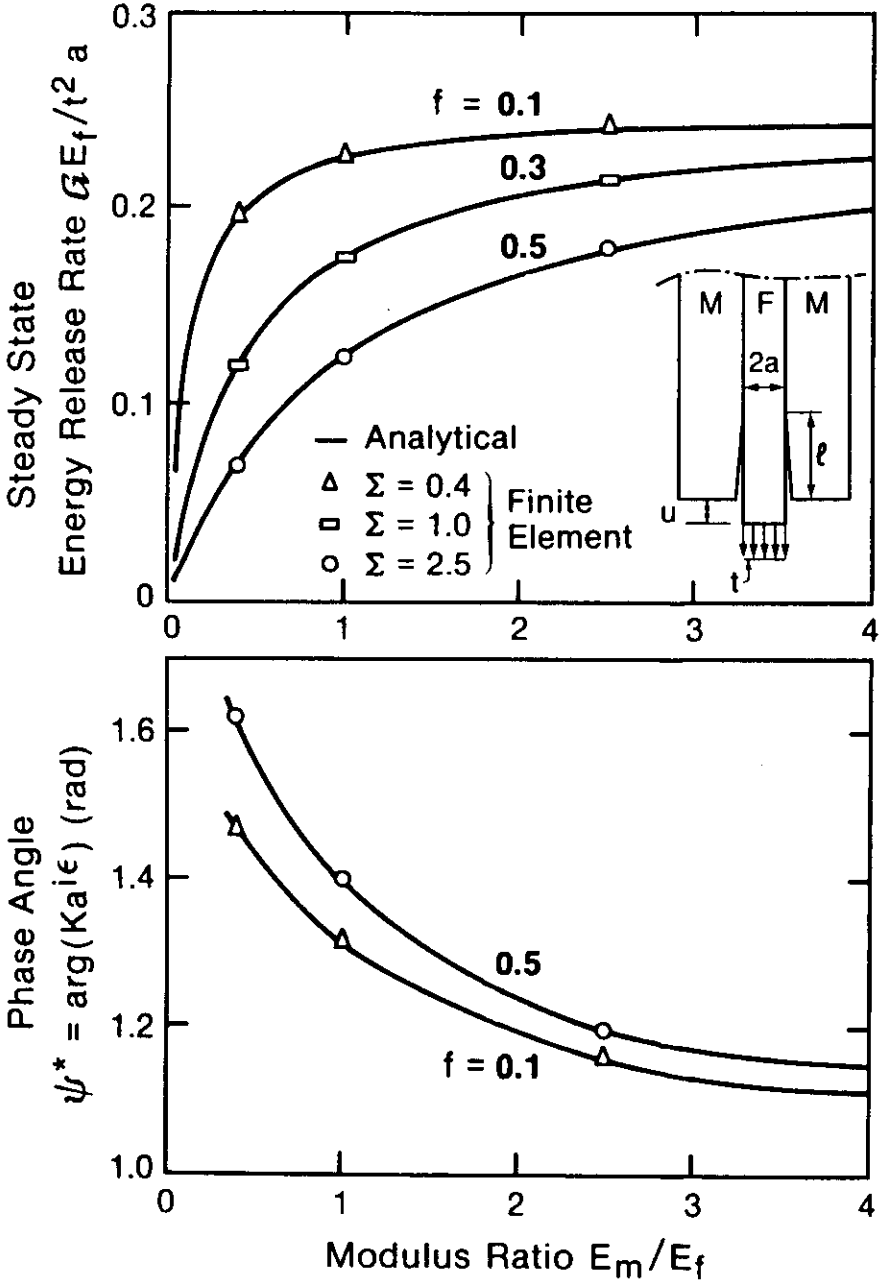
Steady State
Energy Release Rate $\mathcal{G}E_f/t^2\,a$
f = 0.1
0.3
0.5
Analytical
Σ = 0.4
Σ = 1.0
Σ = 2.5
Finite Element
M
F
M
2a
ℓ
u
t
Phase Angle
$\psi^* = \arg(Ka^{i\epsilon})$ (rad)
0.5
f = 0.1
Modulus Ratio E_m/E_f

FIG. 5D

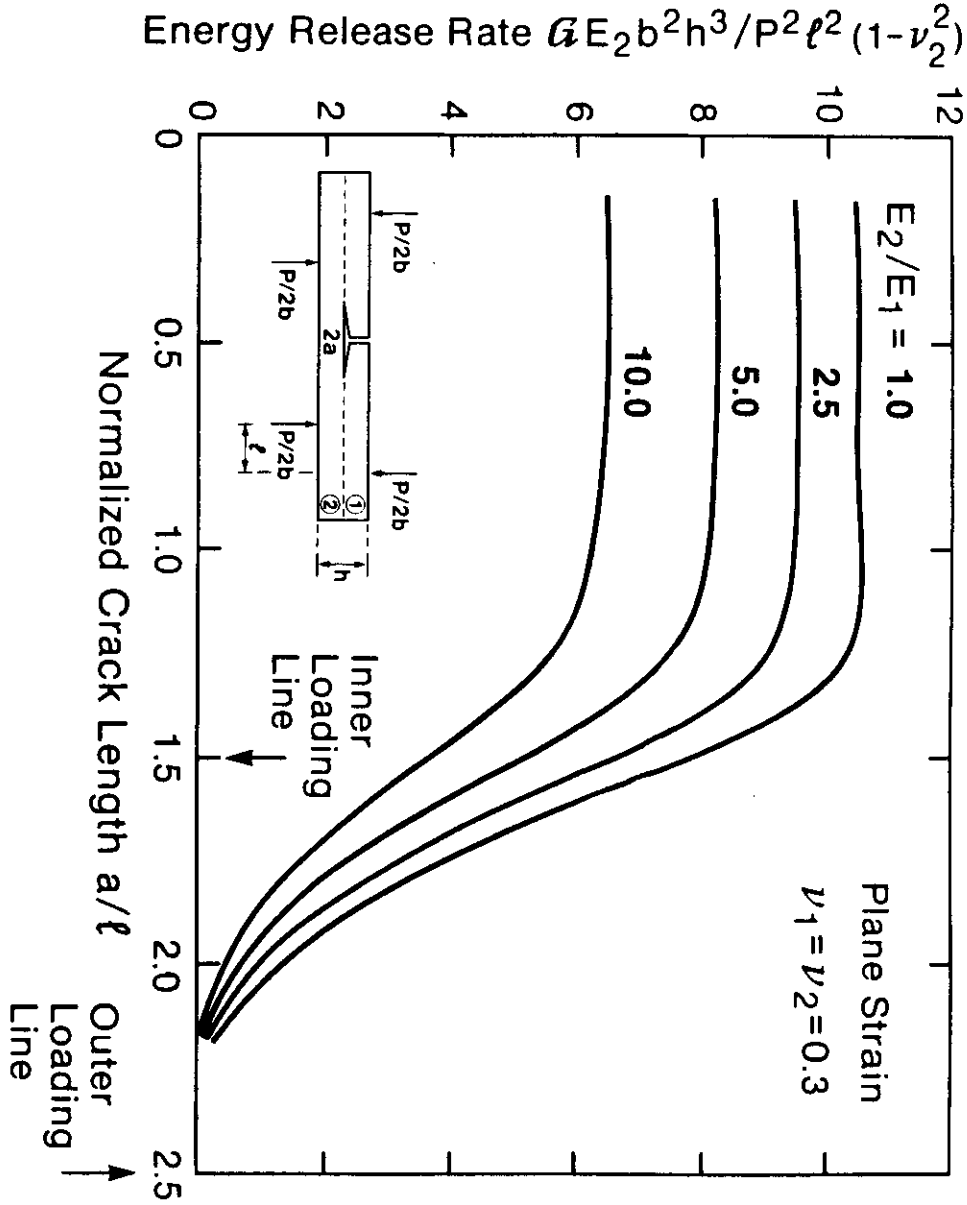
Energy Release Rate $\mathcal{G}E_2b^2h^3/P^2\ell^2(1-\nu_2^2)$
Normalized Crack Length a/ℓ
E_2/E_1 = 1.0
10.0
5.0
2.5
Plane Strain
$\nu_1=\nu_2$=0.3
Inner Loading Line
Outer Loading Line
P/2b
2a
ℓ
h

FIG. 6A

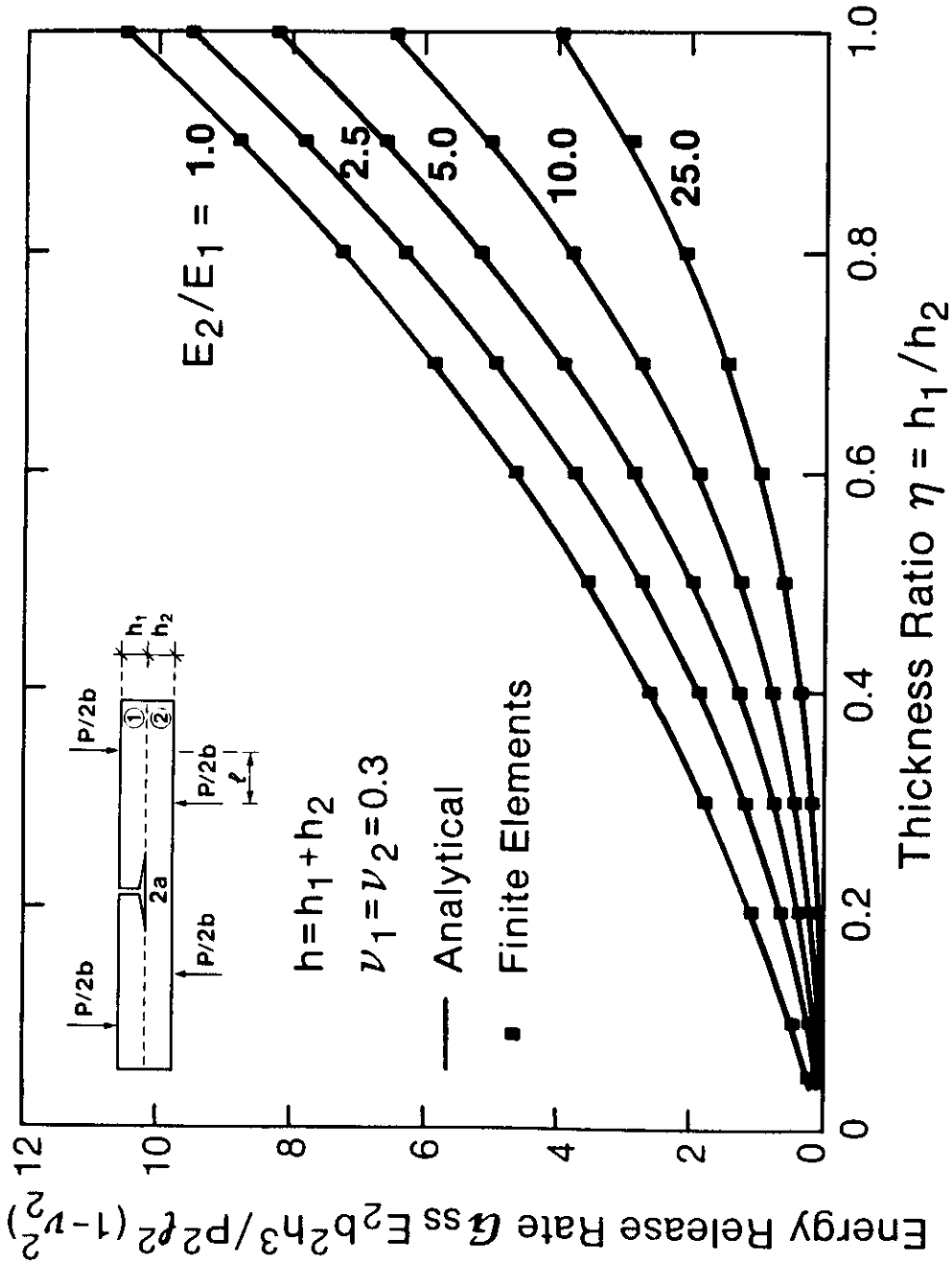
Energy Release Rate $\mathcal{G}_{ss} E_2 b^2 h^3 / P^2 \ell^2 (1-\nu_2^2)$
Thickness Ratio $\eta = h_1/h_2$
$E_2/E_1 = 1.0$
2.5
5.0
10.0
25.0
$h = h_1 + h_2$
$\nu_1 = \nu_2 = 0.3$
Analytical
Finite Elements
P/2b
2a
h_1
h_2
ℓ

FIG. 6B

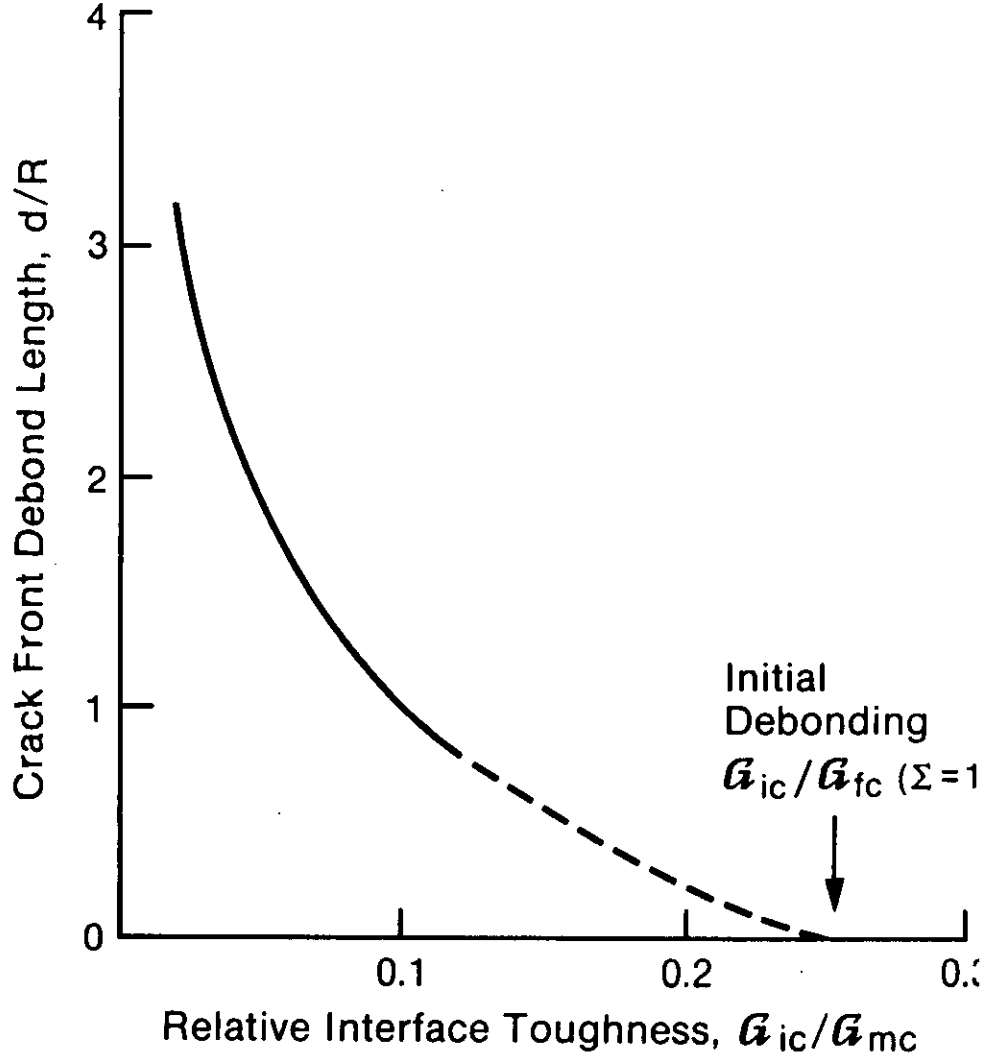
Crack Front Debond Length, d/R
Relative Interface Toughness, $\mathcal{G}_{ic}/\mathcal{G}_{mc}$
Initial
Debonding
$\mathcal{G}_{ic}/\mathcal{G}_{fc}$ (Σ=1

FIG. 7

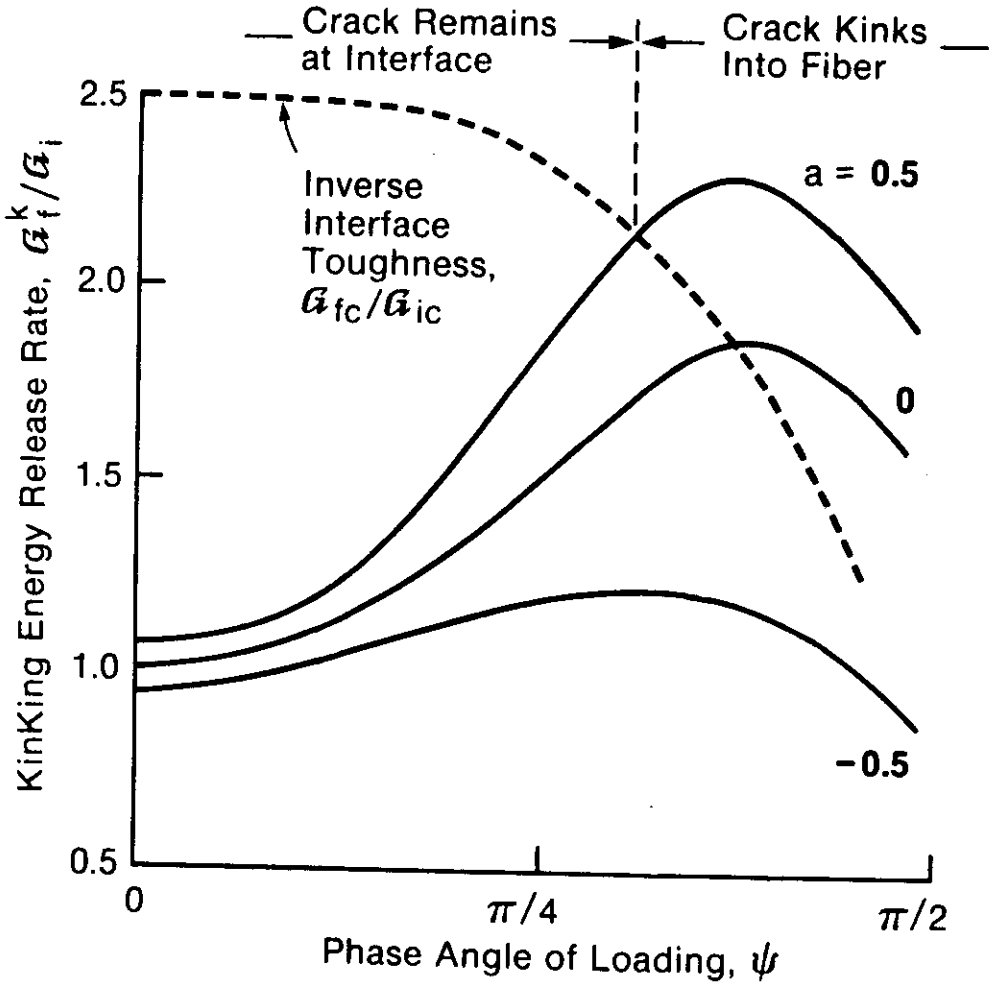
Crack Remains at Interface
Crack Kinks Into Fiber
Inverse Interface Toughness, G_{fc}/G_{ic}
a = 0.5
0
-0.5
KinKing Energy Release Rate, G_f^k/G_i
2.5
2.0
1.5
1.0
0.5
0
$\pi/4$
$\pi/2$
Phase Angle of Loading, ψ

FIG. 8

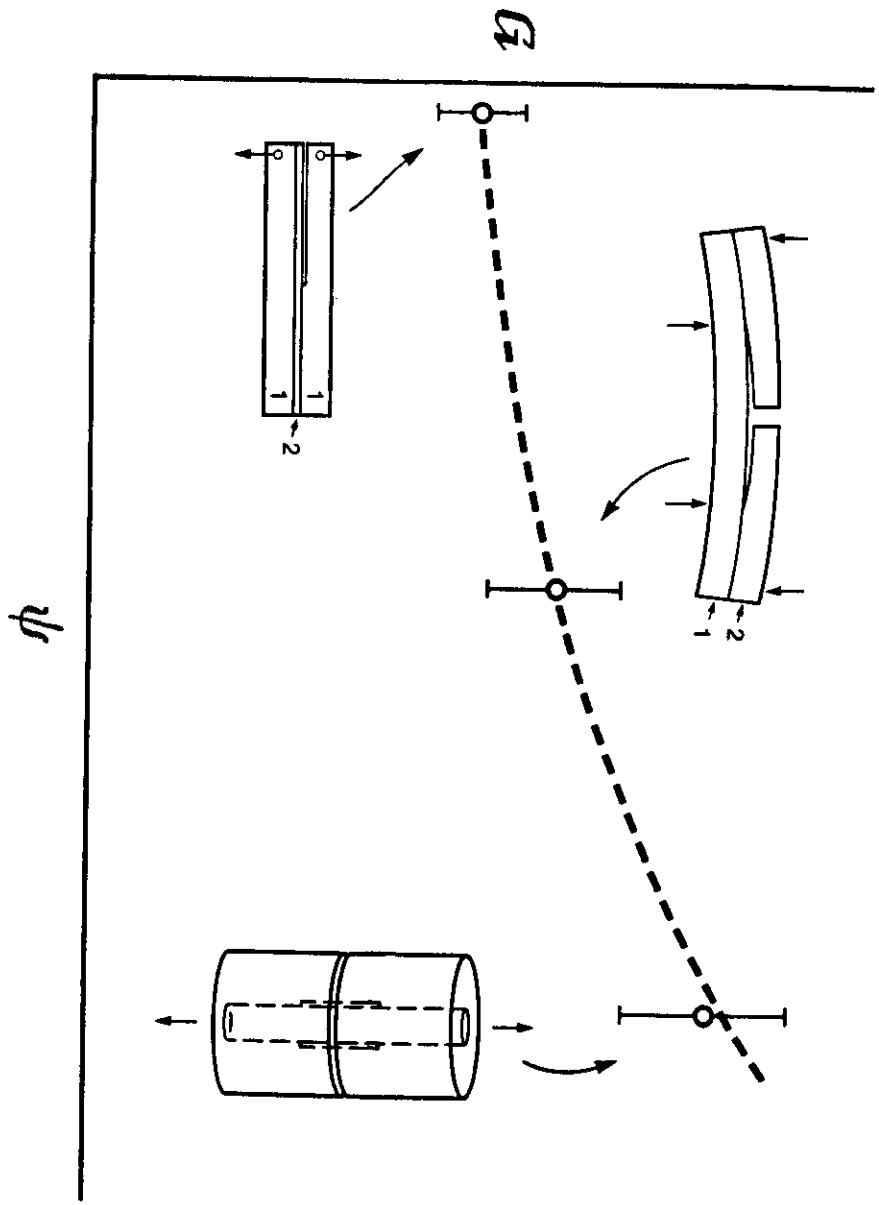
G_1
G_2
1
2
1
1
2

FIG. 9

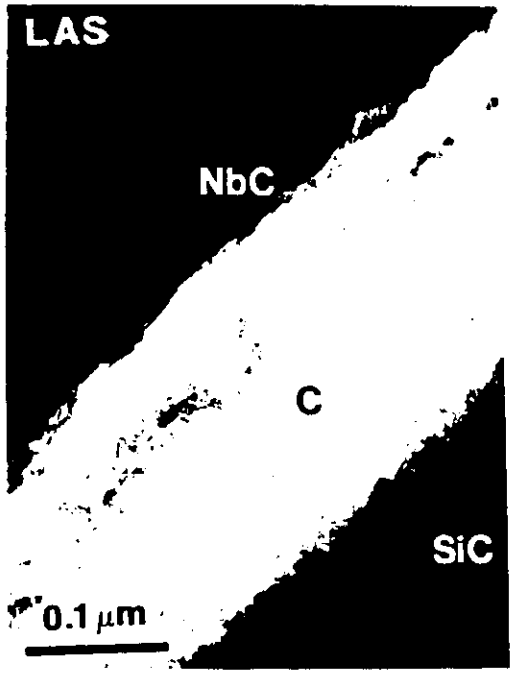

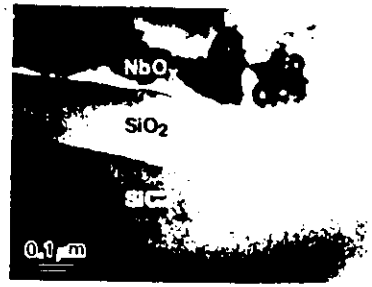

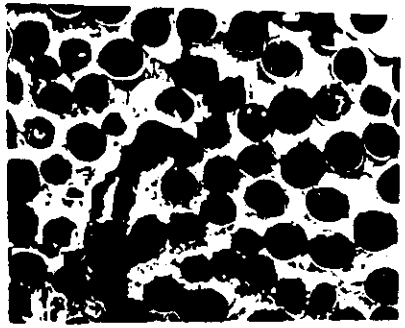

FIG. 10A

FIG. 10B

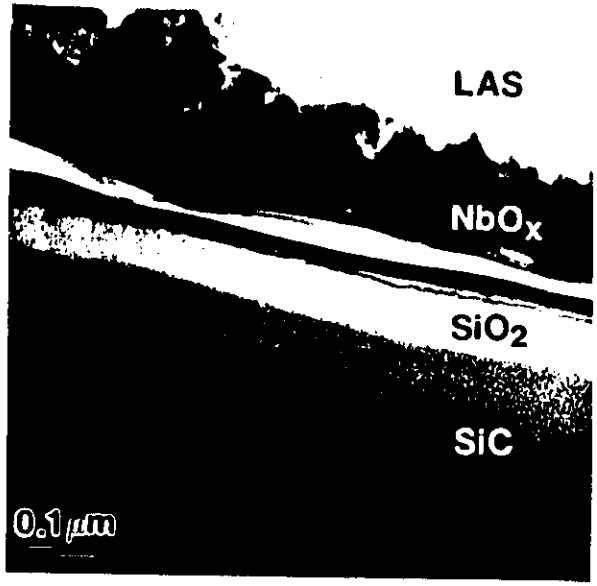
LAS
NbO_x
SiO_2
SiC
0.1 μm

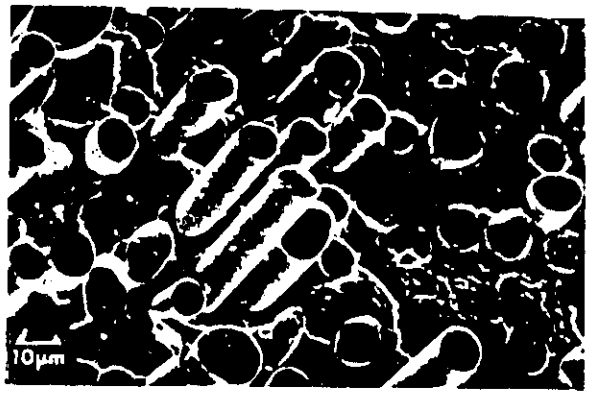
10μm

FIG. 10C

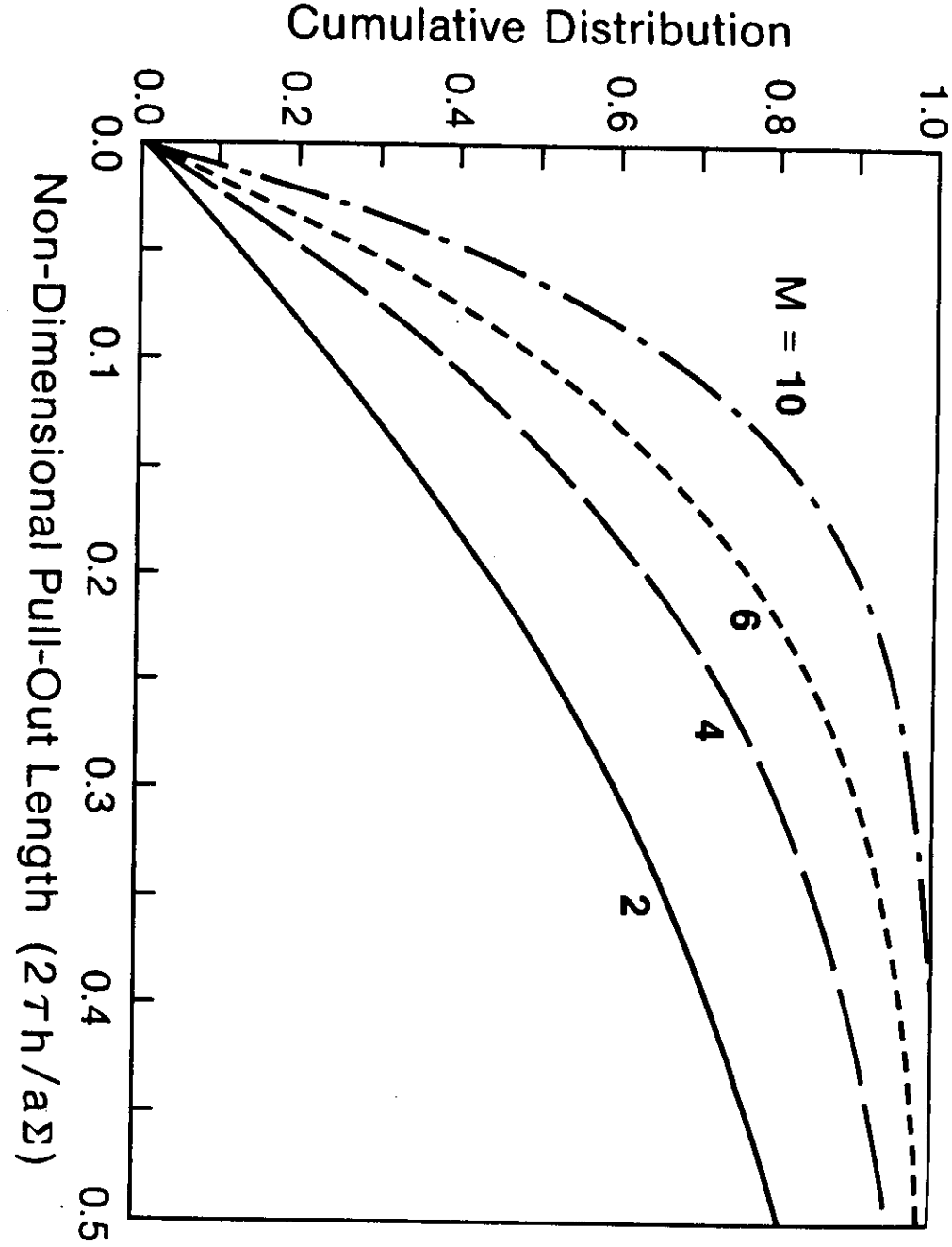
Cumulative Distribution
0.0
0.2
0.4
0.6
0.8
1.0
Non-Dimensional Pull-Out Length ($2\tau h/a\Sigma$)
0.0
0.1
0.2
0.3
0.4
0.5
M = 10
6
4
2

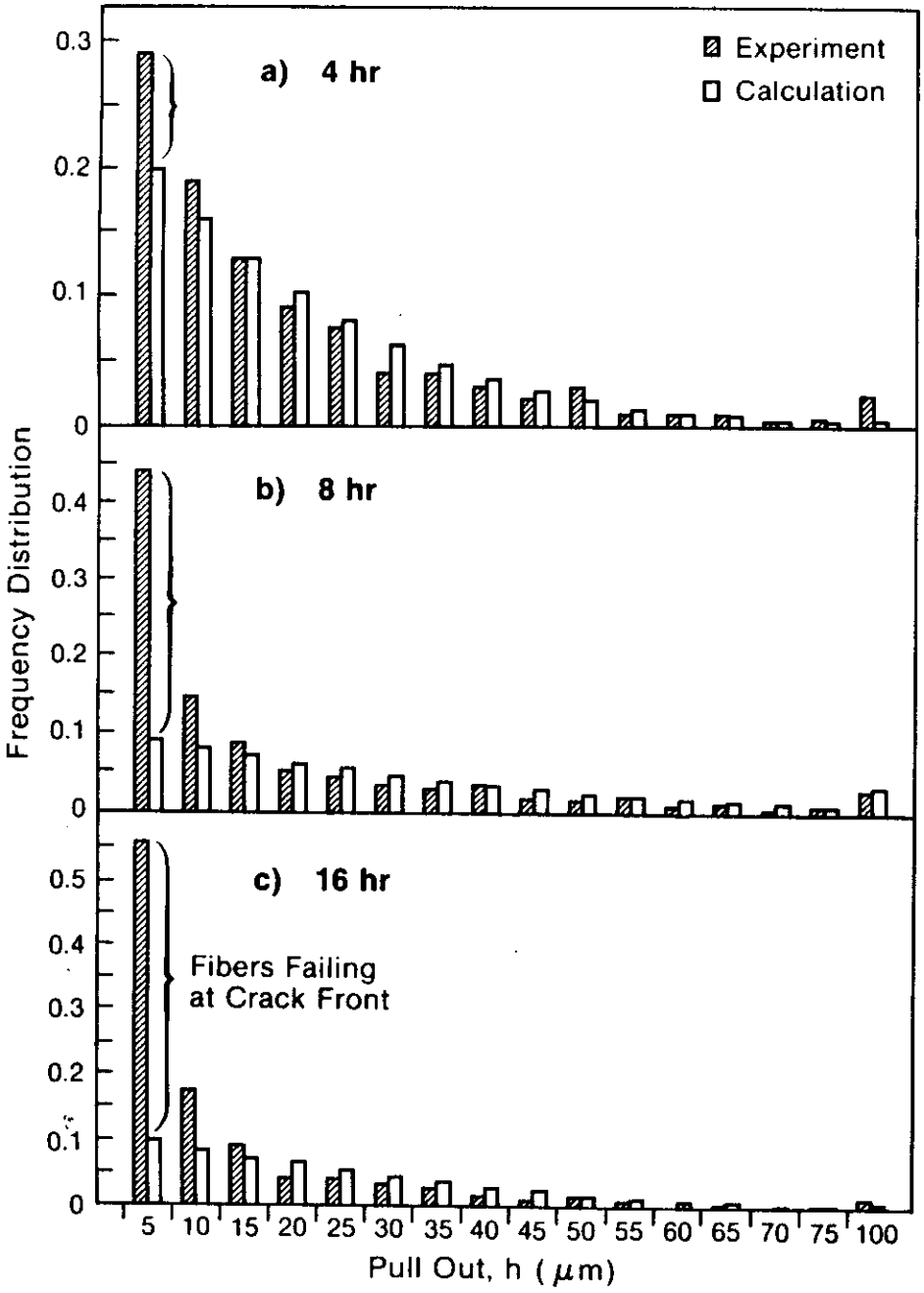

FIG. 12

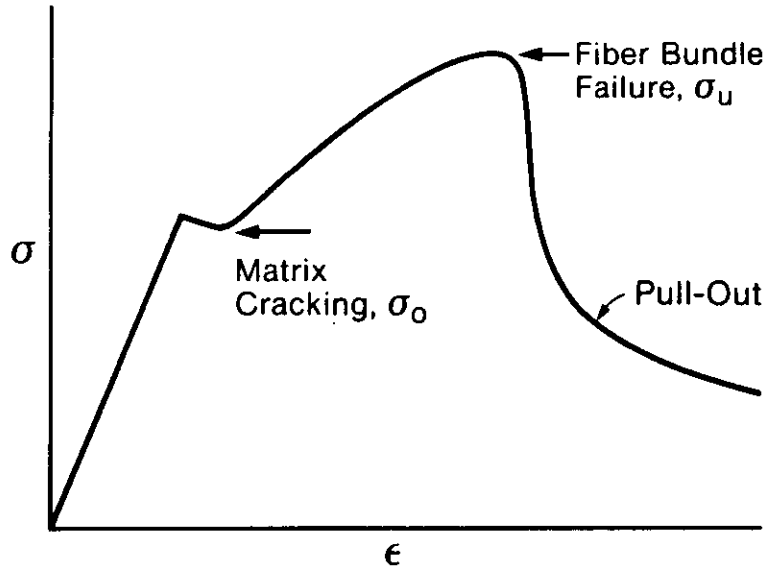

a) 'Tough' Composite

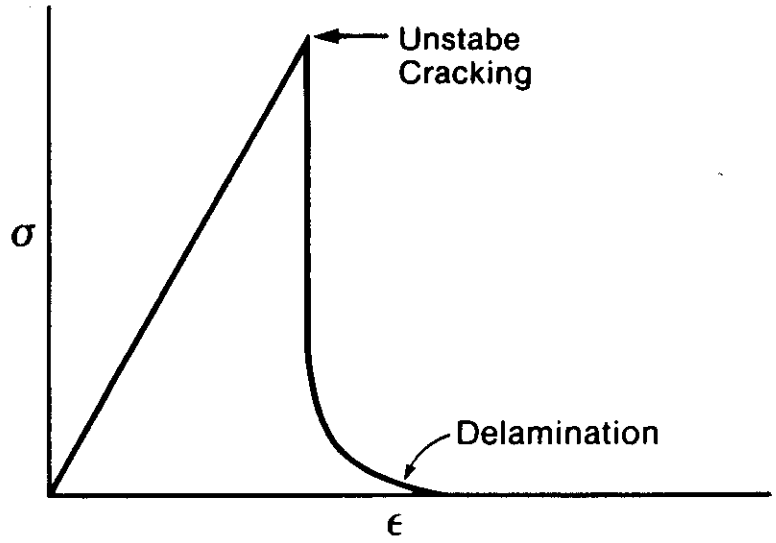

b) 'Brittle' Composite

FIG. 13

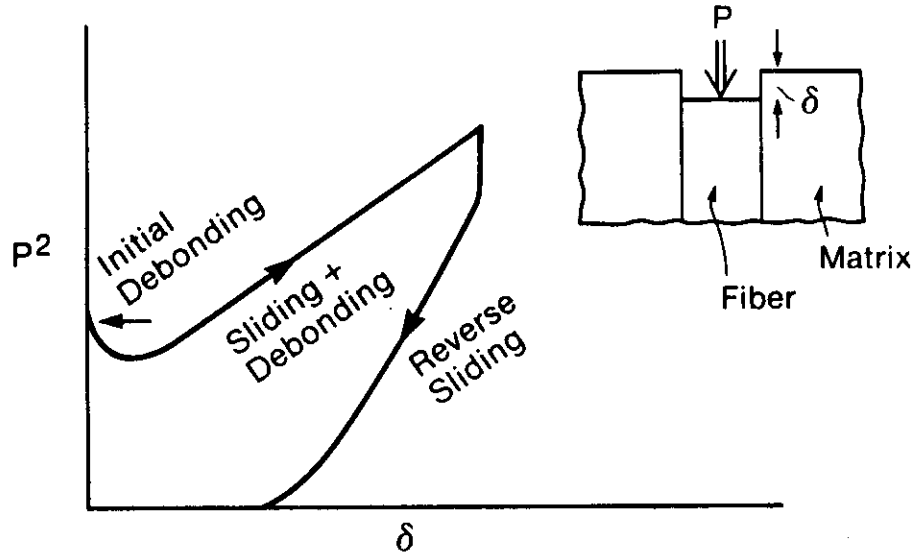

a) Indentation Testing

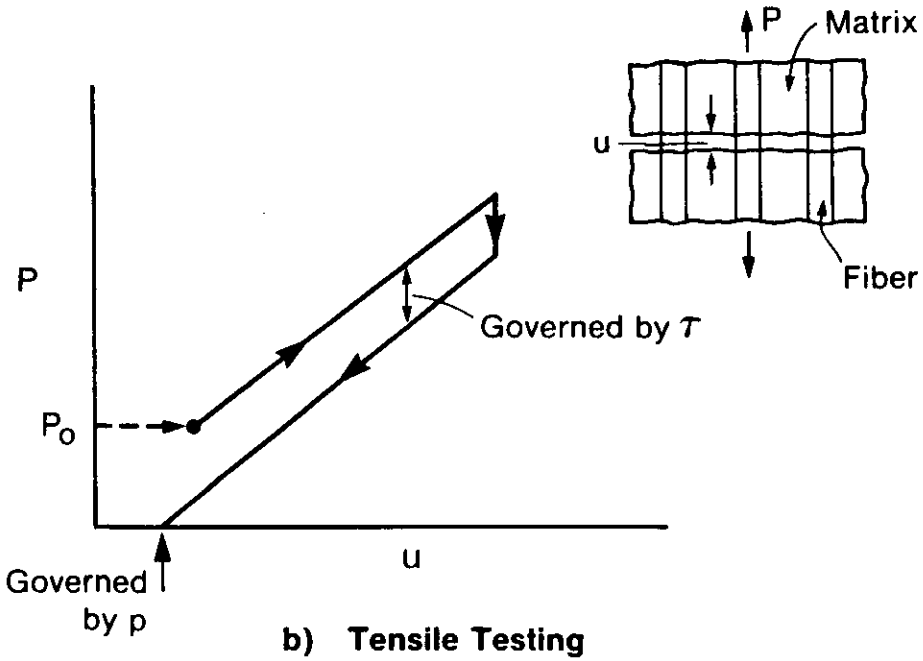

b) Tensile Testing

FIG. 14

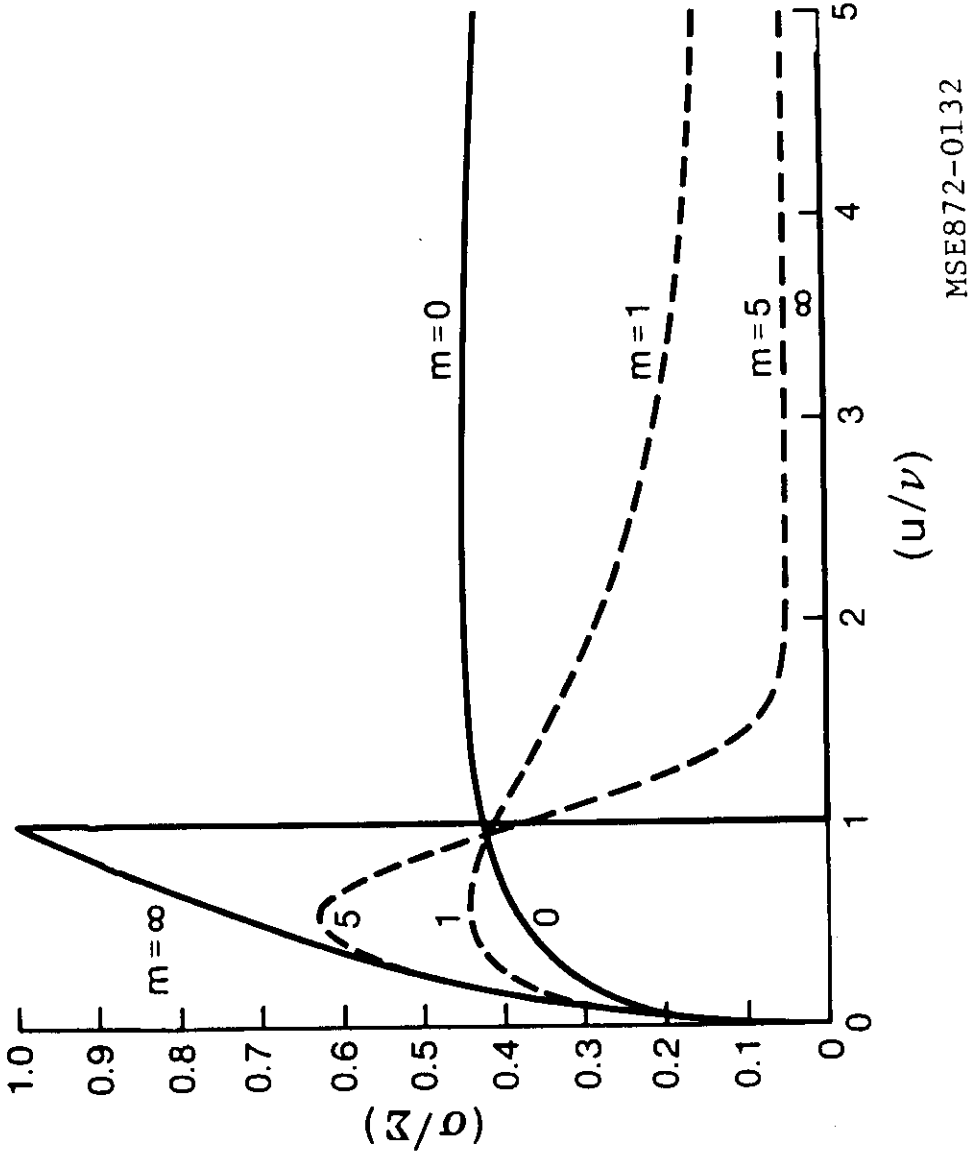

MSE872-0132

FIG. 15

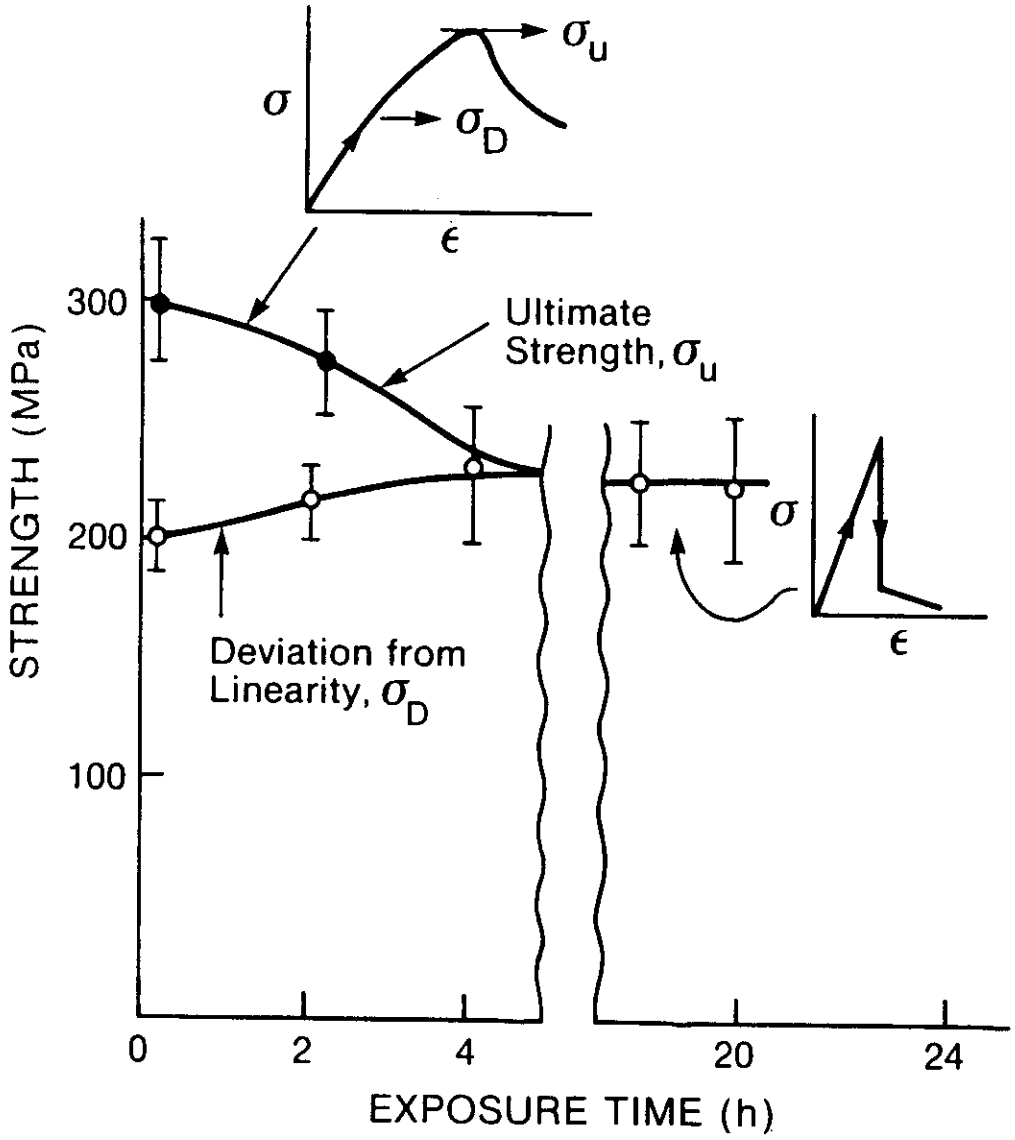
σ_u
σ
σ_D
ϵ
300
200
100
STRENGTH (MPa)
Ultimate
Strength, σ_u
Deviation from
Linearity, σ_D
σ
ϵ
0
2
4
20
24
EXPOSURE TIME (h)

FIG. 16

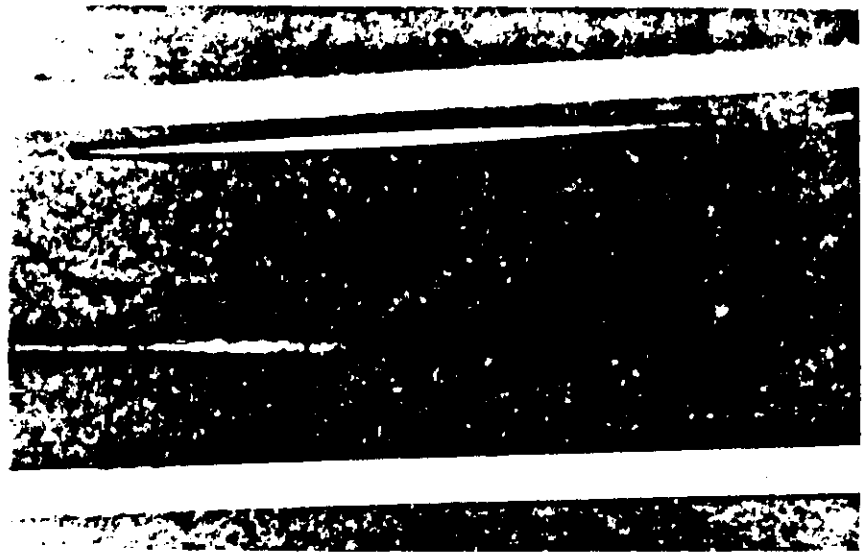

FIG. 17

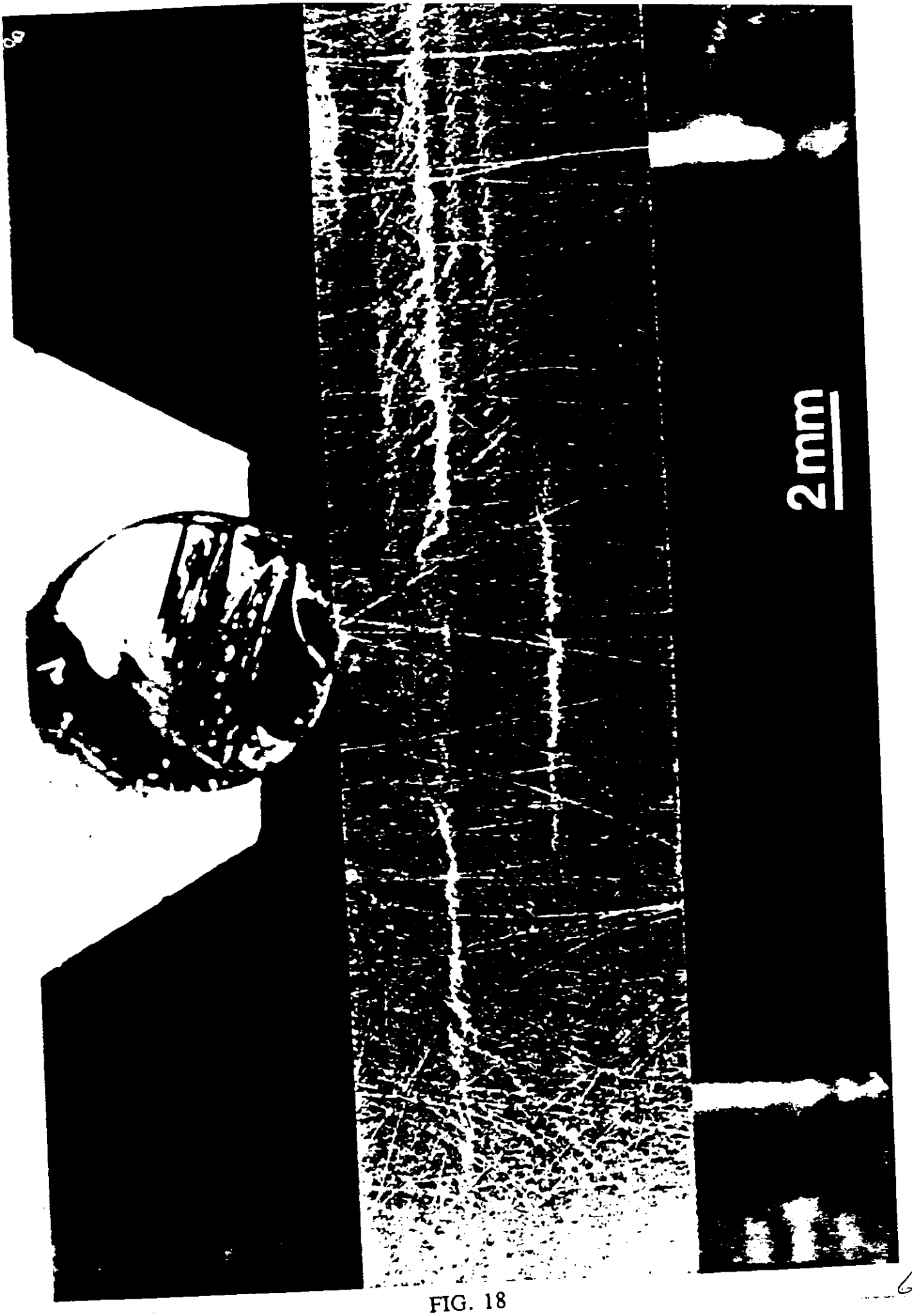

FIG. 18